α5β1 integrin recycling promotes Arp2/3-independent cancer cell invasion via the formin FHOD3

Nikki R. Paul[1], Jennifer L. Allen[1], Anna Chapman[1], Maria Morlan-Mairal[1], Egor Zindy[1], Guillaume Jacquemet[2], Laura Fernandez del Ama[1], Nermina Ferizovic[1], David M. Green[1], Jonathan D. Howe[4], Elisabeth Ehler[3], Adam Hurlstone[1] and Patrick T. Caswell[1,*]

[1] Wellcome Trust Centre for Cell-Matrix Research, Faculty of Life Sciences, University of Manchester, M13 9PT, UK

[2] Present address: Turku Centre for Biotechnology, FIN-20521, Turku, Finland

[3] Randall Division of Cell and Molecular Biophysics, Cardiovascular Division, BHF Research Excellence Centre, New Hunt's House, King's College London, Guy's Campus, London, SE1 1UL, UK

4 Medical Research Council Laboratory of Molecular Biology, Francis Crick Avenue, Cambridge CB2 0QH, United Kingdom

* Author for correspondence:

Patrick T. Caswell, Wellcome Trust Centre for Cell-Matrix Research, Faculty of Life Sciences, University of Manchester, Manchester M13 9PT, UK
Tel.: +44 (0) 161 3060505
Fax: +44 (0) 161 2755082
E-mail: patrick.caswell@manchester.ac.uk
patrick.caswell@manchester.ac.uk

Running title: Actin spikes drive migration in 3D and *in vivo*

Character count: 39, 887

ABSTRACT

Invasive migration in 3D extracellular matrix (ECM) is crucial to cancer metastasis, yet little is known of the molecular mechanisms that drive reorganisation of the cytoskeleton as cancer cells disseminate *in vivo*. 2D Rac-driven lamellipodial migration is well understood, but how these features apply to 3D migration is not clear. We find that lamellipodia-like protrusions and retrograde actin flow are indeed observed in cells moving in 3D ECM. However, Rab-coupling protein (RCP)-driven endocytic recycling of $\alpha5\beta1$ integrin enhances invasive migration of cancer cells into fibronectin-rich 3D ECM, driven by RhoA and filopodial spike-based protrusions, not lamellipodia. Furthermore, we show that actin spike protrusions are Arp2/3-independent. Dynamic actin spike assembly in cells invading *in vitro* and *in vivo* is regulated by Formin homology-2 domain containing 3 (FHOD3), which is activated by RhoA/ROCK, establishing a novel mechanism through which the RCP/$\alpha5\beta1$ pathway reprograms the actin cytoskeleton to promote invasive migration and local invasion *in vivo*.

INTRODUCTION

Malignant transformation and metastatic spread is the main cause of death in cancer patients. In order to metastasise, cells must acquire the ability to migrate and invade in 3D matrices, requiring dynamic reorganisation of the actin cytoskeleton to alter morphology and provide protrusive force (Bravo-Cordero et al., 2012). Cancer cells are understood to adopt a range of migratory strategies, from collective to single cell invasion, and the mechanisms that drive protrusion are thought to be dictated by RhoGTPases (Sanz-Moreno et al., 2008). For example, the leader cells in collective invasion and single 'mesenchymal' cells migrate in a Rac-dependent manner (Friedl and Alexander, 2011; Friedl et al., 2012; Bravo-Cordero et al., 2012; Theveneau and Mayor, 2013), with the mechanisms of actin polymerisation, protrusion and force generation thought to be reliant on Arp2/3, analogous to lamellipodial migration in 2D (Law et al., 2013; Giri et al., 2013; Krause and Gautreau, 2014). Lamellipodium-independent 3D migration strategies have also been described. Single cells can adopt an 'amoeboid' migration strategy, similar to the movement of leukocytes, whereby RhoA/ROCK activity promotes actomyosin contractility and membrane blebbing to provide protrusive force (Friedl and Alexander, 2011), and lobopodial migration is driven by RhoA/ROCK-mediated contractility providing the force to drive nuclear pistoning (Petrie et al., 2012, 2014). Both of these mechanisms require actomyosin contractility at the rear of the cell to drive an increase in hydrostatic pressure and forward movement of the cell in the absence of actin polymerisation-dependent protrusive structures. We have recently shown that RCP-mediated $\alpha5\beta1$ recycling locally activates RhoA at the cell front to promote formation of pseudopodial protrusions tipped by actin spikes (Jacquemet et al., 2013a). However, an understanding of how the molecular mechanisms underlying lamellipodial protrusion in 2D

are reflected in 3D, and how non-lamellipodial actin-based protrusions are dynamically regulated in 3D, is lacking.

Integrins are α/β heterodimeric receptors that mediate communication between the cell and the extracellular matrix (ECM), capable of eliciting a plethora of signalling responses to effect a host of functional outcomes (Hynes, 2002; Legate et al., 2009; Ivaska and Heino, 2011). Although integrins alone are not oncogenic, dysregulation of integrin signalling is frequently a prognostic indicator of tumour progression (Desgrosellier and Cheresh, 2010). For example, in high grade ovarian tumours αvβ3 integrin expression is downregulated (Maubant et al., 2005) and patients with high β3 integrin expression have an improved prognosis (Kaur et al., 2009), whereas high expression of α5β1 integrin is an indicator for poor outcome (Sawada et al., 2008).

The endocytic trafficking of integrins plays an important role in regulating integrin function during cell division and migration (Caswell and Norman, 2006; Pellinen and Ivaska, 2006; Caswell et al., 2009; Bridgewater et al., 2012; Jacquemet et al., 2013b), in particular the recycling of the fibronectin (FN) receptor α5β1 promotes invasive migration in 3D ECM (Caswell et al., 2007, 2008; Caswell and Norman, 2008; Muller et al., 2009; Dozynkiewicz et al., 2012) Rab coupling protein (RCP, Rab11-FIP1) can interact with α5β1 to control its recycling; inhibition of αvβ3 integrin (with small-molecule inhibitors, e.g. cilengitide, cRGDfV, or soluble ligands e.g. osteopontin), or expression of gain-of-function mutant p53 (e.g. R273H, R175H) promotes the association of RCP with α5β1 and leads to rapid recycling of this integrin (Caswell et al., 2008; Muller et al., 2009). RCP/α5β1 vesicles accumulate in protrusive pseudopods in 3D matrix, driving their extension and resulting in invasive migration (Caswell et al., 2008; Rainero et al., 2012). Rather than directly influence the adhesive capacity of the cell, RCP-driven α5β1 recycling coordinates signalling of receptor tyrosine kinases (RTKs,

including EGFR1, c-Met; Caswell et al., 2008; Muller et al., 2009) to drive polarised signalling within the tips of invasive pseudopods through the RacGAP1-IQGAP1 complex. This leads to local suppression of activity in the small GTPase Rac1 and increased activity of RhoA, which drives extension of long pseudopodial processes tipped with actin spikes at the cell front, as opposed to formation of wave-like structures, enabling subsequent migration and invasion in 3D ECM (Jacquemet et al., 2013a).

Reorganisation of the actin cytoskeleton to promote actin-based protrusion requires actin filament elongation, catalysed by actin assembly factors that promote nucleation and/or elongation of actin filaments (Krause and Gautreau, 2014; Nürnberg et al., 2011). The Arp2/3 complex polymerises actin filaments as branches from existing filaments, generating a complex, dense and highly branched network of actin filaments, such as that seen within the lamellipodium of cells migrating in 2D (Krause and Gautreau, 2014). Actin polymerisation within the lamellipodium pushes filaments against the membrane at the leading edge and this force, combined with actomyosin contractility, generates retrograde flow of actin filaments and complexes associated with the actin network (Lai et al., 2008). Some of these rearwards-sliding actin filaments are captured by integrin adhesion complexes that form within the lamellipodium; this acts as a 'molecular clutch' to transfer retrograde actin flow into protrusive traction force, driving the lamellipodium forward (Gardel et al., 2008; Thievessen et al., 2013). Filopodia are an alternate class of protrusion found at the leading edge of migrating cells that can be generated through Arp2/3-dependent (convergent elongation) and -independent (tip nucleation) means of actin polymerisation (Mattila and Lappalainen, 2008; Mellor, 2010). Filopodia contain more stable F-actin bundles, and rates of protrusion and retrograde flow are inversely correlated (Mallavarapu and Mitchison, 1999). Formins promote the formation of unbranched actin filaments, by nucleating actin

polymerisation at the barbed end processively and promoting elongation by resisting capping (Mattila and Lappalainen, 2008; Mellor, 2010; Nürnberg et al., 2011). Diaphanous-related formins (DRFs) are effectors for RhoGTPases, which bind to DRFs to relieve the autoinhibitory interaction between the diaphanous inhibitory domain (DID) and the diaphanous autoregulatory domain (DAD), and have been reported to play a role in filopodia formation and contribute to lamellipodial extension (Peng et al., 2003; Pellegrin and Mellor, 2005; Block et al., 2012). The DRFs FMNL2 and FMNL3 have further been shown to play a role in migration in 3D matrix (Kitzing et al., 2010; Vega et al., 2011), although how they contribute to actin-based protrusion is currently unclear.

In the present study, we have interrogated the dynamics of actin-based protrusion in migrating and invading carcinoma cells. We find evidence of retrograde flow in wave-like lamellipodial protrusions in 3D matrix; however upon increasing the invasive capacity of cells by promoting RCP/α5β1 trafficking we observe more stable long filopodia which form actin spike protrusions. RCP/α5β1 trafficking increased local invasion of cancer cells *in vivo*, where cells exhibit dynamic actin spike protrusions. Furthermore, we show that formation of actin spikes is Arp2/3-independent, but requires ROCK-mediated phosphorylation and activation of the DRF Formin homology domain 2 containing 3 (FHOD3). Finally, FHOD3 is required for local invasion *in vivo*, downstream of RCP/α5β1 trafficking, providing evidence that integrin trafficking dictates a novel actin polymerisation program to promote actin spike protrusion formation and invasion in 3D microenvironments.

RESULTS

RCP/α5β1 integrin trafficking alters F-actin dynamics in cell protrusions

Retrograde flow of actin filaments is a feature of lamellipodial migration, which when coupled to integrin adhesion complexes, provides a powerful force driving forward movement of cells (Gardel et al., 2008; Lai et al., 2008; Thievessen et al., 2013). We employed a photoactivation approach in cells expressing photoactivatable GFP- (paGFP-) actin and Lifeact-mRFPmars in combination with spinning disk confocal microscopy to analyse retrograde actin flow in carcinoma cell lines migrating on 2D surfaces. Upon activation of paGFP-actin within a small region (5μm^2) at the leading edge of the lamellipodium, evidence of retrograde flow could be seen in A2780 ovarian cancer cells and H1299 non-small cell lung cancer cells, as a pool of photoactivated paGFP-actin dissipated from the photoactived region at a slower rate than freely diffusible paGFP and passed through a region of interest immediately behind that activated within approximately 30 seconds (Figure S1A, B).

We have previously shown that RCP/α5β1-dependent trafficking, induced by inhibition of αvβ3 integrin (using cRGDfV, a selective cyclic peptide inhibitor of αvβ3 integrin) or mutant p53 expression, promotes the formation of dynamic actin-rich protrusions which actively ruffle to promote rapid but less directionally persistent migration in 2D (Caswell et al., 2008; Muller et al., 2009). Upon activation of paGFP-actin within dynamically ruffling protrusions, the lower rate of diffusion of paGFP-actin away from the photoactivated region suggested that these structures were more stable, but retrograde flow of actin filaments was also slowed as a lower level of photoactivated paGFP-actin dispersed through the region immediately behind that photoactivated (Figure S1A, B).

Whilst there is evidence that Rac, and downstream effector pathways leading to activation of Arp2/3 (Sanz-Moreno et al., 2008; Giri et al., 2013; Law et al., 2013), plays a role

in 3D migration, there is little evidence to suggest that the mechanism that drives lamellipodial traction force in 3D ECM is linked to retrograde actin flow. We seeded carcinoma cells onto cell-derived matrix (CDM), a linearly elastic 3D matrix made up of fibrillar collagen and fibronectin (Cukierman et al., 2001; Petrie et al., 2012, 2014). Under basal conditions, A2780 cells formed wave-like protrusions resembling small lamellipodia towards the cell front (reflecting Rac activity localised in this subcellular region; Jacquemet et al., 2013a), structures that have been noted previously in different cell lines in 3D ECM (Petrie et al., 2012; Giri et al., 2013; Jacquemet et al., 2013a). Upon activation of paGFP-actin at the leading edge of these protrusive structures, retrograde flow of actin was clearly observable within the region immediately behind that activated (Figure 1A, B, C, Movie 1), with similar kinetics to those observed in 2D. Interestingly, when RCP/α5β1 trafficking was induced with cRGDfV, protrusions again appeared more stable, and F-actin structures showed slower rates of retrograde flow (Figure 1A, B, C, Movie 1). Moreover, the dynamics of paGFP-actin in MDA-MB-231 cells, which express an endogenous gain-of-function mutant p53, suggest that these cells generate F-actin protrusions that are not subjected to rapid retrograde flow in FN-rich ECM (Figure S1C). These data suggest that RCP/α5β1 integrin-driven actin-based protrusions are relatively stable and exhibit low rates of retrograde flow.

Promoting RCP/α5β1 trafficking leads to the formation of F-actin spikes and increased invasion *in vivo*

RCP/α5β1 integrin trafficking leads to an increase in F-actin density at protrusions of cells migrating in 3D CDM or high concentration collagen/FN hydrogels (Jacquemet et al., 2013a). Live-cell spinning disk imaging, capturing z-stacks of A2780 cells transfected with Lifeact-mEGFP migrating in CDM over timecourses that expose protrusive events, revealed

small, wave-like protrusions under basal conditions which, like 2D lamellipodia, were made up of F-actin veils between filopodia (Figure 1D, Movie 2). Upon addition of cRGDfV to promote RCP/$\alpha5\beta1$ recycling, cells migrating in 3D CDM formed larger actin spike-based protrusions (Figure 1E, Movie 2). Using an unbiased analysis to mask protrusions at the front of migrating cells over many frames (Figures 1F, G), we found that RCP/$\alpha5\beta1$ trafficking generates larger protrusive areas (Figure 1H). H1299-Vec cells, which move with broad lamellipodia in 2D (Figure S1B, Muller et al. 2009), possess wave-like lamellipodia in 3D CDM, however, upon expression of mutant p53 in H1299 cells, dynamic bursts of spike-like structures were observed (Figure S2A, B). Similarly, MDA-MB-231 cells also displayed intense clusters of actin spikes, which were concentrated at cell protrusions in the direction of cell migration (Figure S2C). Structured illumination microscopy (SIM) enabled the resolution of bundled F-actin filaments within protrusions as cells move in 3D CDM, to reveal the switch from predominantly lamellipodial protrusion to an increase in the number and length of filopodia at the tips of invasive pseudopods upon induction of RCP/α5β1 trafficking with cRGDfV (Figure 1I-K). Live imaging further demonstrated that filopodial lifetime was also increased in cRGDfV treated cells (Figure S2D). These data suggest that, in several carcinoma cells lines, signalling downstream of RCP/α5β1 trafficking suppresses lamellipodia formation and promotes formation of filopodia which are arranged into F-actin spikes in the direction of migration in 3D CDM.

We have previously demonstrated that RCP-driven recycling of α5β1 and co-cargo RTKs, induced by inhibition of αvβ3 integrin or mutant p53 expression, leads to increased invasion into FN-rich ECM (Caswell et al., 2008; Muller et al., 2009, 2013), and gain-of-function mutant p53 promotes metastasis in genetically engineered mouse models (Caulin et al., 2007; Adorno et al., 2009; Muller et al., 2009; Doyle et al., 2010; Arjonen et al., 2014). We sought

to determine whether manipulation of α5β1 integrin trafficking could influence local invasion in a physiologically relevant *in vivo* environment, a zebrafish xenograft model in which melanoma cells have been shown to disseminate in association with collagen and FN (Chapman et al., 2014). Under basal conditions, cells formed a xenograft tumour mass in the pericardial cavity, but showed negligible signs of dissemination through surrounding tissue (Figure 2A, C, D, F). Upon addition of cRGDfV (A2780 cells) or expression of mutant p53 R273H (H1299 cells) a significant increase in the ability of cells to locally invade into the jaw region of the embryo was observed (Figure 2B, C, E, F), suggesting that promoting RCP/α5β1 trafficking increases the capacity of cells to invade an *in vivo* tissue environment.

Casper strain zebrafish are amenable to imaging, so we next investigated the dynamics of F-actin protrusions in cells invading *in vivo*. A2780 cells stably expressing Lifeact-mRFPmars were injected into zebrafish embryos and allowed to invade for 48 hours before live spinning disk confocal imaging. Invading cells possessed large spike-like F-actin protrusions in the direction of invasion (Figure 2G-I), which appeared larger and thicker structures than those observed in cells migrating *in vitro*, but clearly showed dynamic actin polymerisation and depolymerisation (Figure 2I, Movie 3). Together these data reveal that RCP-driven α5β1 integrin trafficking leads to the formation of filopodia and actin spikes (but not lamellipodia or membrane blebs) and local invasion *in vivo*.

The Arp2/3 complex is not required for RCP/α5β1-driven actin polymerisation and invasive migration

We next sought to identify potential downstream effectors of the RCP/α5β1 integrin pathway that lead to altered morphology and dynamics of actin-based protrusion. CK-666, an Arp2/3 inhibitor (Nolen et al., 2009), caused lamellipodia to collapse under basal

conditions in 2D, whereas the inactive analogue CK-689 had no effect (Figure S3A). However, CK-666 treated cells were able to form protrusions in the direction of migration, similar to actin-rich ruffling protrusions which form in response to RCP/α5β1 trafficking (Figure S1A; Caswell et al., 2008) and knockdown of ArpC2 or ArpC3 (Figure 3A). CK-666 treated A2780 cells moved in a rapid but less directionally persistent manner (Figure S3B-E), similar to the 2D migratory phenotype observed upon induction of RCP-driven α5β1 recycling (+cRGDfV), whilst migration of mouse embryonic fibroblasts was impaired by these concentrations of CK-666 (Figure S3F) as previously observed (Wu et al., 2012). Moreover, Arp2/3 inhibition had no significant influence on 2D migration in the presence of cRGDfV (Figure S3B-E). RCP/α5β1-driven morphology and migration in 3D CDM was unaffected by ArpC2 and ArpC3 knockdown (Figure 3B-D, S3H-J) or Arp2/3 inhibition (Figure 3F, G, S3G), and under basal conditions these interventions did not influence migration (Figure 3C, F, G, S3G, I), but ArpC2 knockdown and CK-666 treated A2780 cells appeared to extend longer pseudopodial protrusions (Figure 3D, H, S3J). Interestingly, Arp2/3 inhibition did not abrogate the recycling of $\alpha5\beta1$, and in fact induced a modest increase in recycling under basal conditions (Figure S3K). Furthermore, inhibition of Arp2/3 promoted the accumulation of RCP-containing vesicles to pseudopod tips (Figure S3L, M), suggesting that Arp2/3 could oppose RCP/$\alpha5\beta1$ trafficking. These data indicate that in cancer cells Arp2/3 is not always required for migration, and may even supress RCP/$\alpha5\beta1$-driven signalling to the cytoskeleton and filopodial actin spike formation.

Live imaging of A2780 cells expressing Lifeact-mEGFP showed that cells treated with cRGDfV were still able to generate large, filopodia-based protrusions upon addition of CK-666 and CK-689 (Figure 3E, H, Movie 4). Furthermore, Arp2/3 inhibition had no significant influence on the very low basal level of A2780 cell invasion, nor did it affect RCP/α5β1-driven invasion into plugs of FN-rich fibrillar collagen (Figure 3I). Together these data suggest that

RCP/α5β1-driven protrusion, migration and invasion is not reliant on Arp2/3-mediated actin polymerisation, suggesting that other pathways influence actin dynamics in this context.

Formin inhibition abrogates invasive migration

Formins are a family of 15 actin nucleators which drive processive polymerisation of actin filaments from the barbed end, some of which can act as RhoGTPase effectors (DRFs, Mellor, 2010; Nürnberg et al., 2011). The pan-formin inhibitor SMIFH2 (Rizvi et al., 2009) profoundly abrogated protrusion formation in cells migrating in 3D CDM (Figure 4A, B) and invasion into collagen/FN-rich ECM (Figure 4D), and cells instead formed membrane blebs (Figure 4A, C), suggesting that formins mediate actin reorganisation within protrusions as cells migrate in 3D ECM.

FHOD3 is specifically required for RCP/α5β1 integrin-driven actin dynamics and migration

Of the 15 mammalian formins, 12 were found to be expressed at relatively high levels in A2780 cells (Figure 4E). Because the function of inverted formins (INF1/2) in actin polymerisation is less well defined, we knocked down the remaining 10 formins (Figure S4A) and measured migration speed of cells in 3D CDM. In cells migrating in an RCP/α5β1-dependent manner, knockdown of the formin like family (FMNL, in particular FMNL2, FMNL3) and FHOD3 significantly decreased migration speed (Figure 4F). However, FHOD3 knockdown did not affect migration speed under basal conditions (Figure 4G), suggesting that this DRF could function specifically downstream of the RCP/α5β1 integrin pathway.

Confirming the siRNA miniscreen, stable knockdown of FHOD3 reduced RCP/α5β1-driven (but not basal) migration and suppressed pseudopod extension in A2780 cells in 3D CDM (Figure 5A-D, S4B), but had no discernible influence on cell migration in 2D (Figure S4C-

E), and the effect of FHOD3 knockdown on 3D migration was rescued by re-expression of shRNA resistant RFP-FHOD3; in fact RFP-FHOD3-expressing cells migrated significantly faster (Figure 5B, S4F). The cell lines used in this study expressed only the non-muscle specific isoform of FHOD3 (Figure S4G), and this isoform was used for rescue experiments.

RFP-FHOD3 showed a punctate distribution throughout the cytoplasm of cells in 3D CDM, sometimes decorating F-actin bundles under basal conditions but with little localisation at the leading edge (Figure S5A). Upon induction of RCP/ α5β1 trafficking, cells generated numerous filopodial protrusions at the leading edge, and RFP-FHOD3 puncta could be seen within these actin spike protrusions, whereas RFP alone was diffuse (Figure S5A). Interestingly, a constitutively active mutant of FHOD3, which lacks the DAD domain (GFP-FHOD3ΔDAD), promoted formation of spike-like actin protrusions, and accumulated at these structures (Figure S5B, C), suggesting that FHOD3 could directly influence the formation of filopodia and actin spikes in invading cells. Live-cell imaging of Lifeact-mTFP1-expressing FHOD3 knockdown cells revealed non-apoptotic membrane blebs at the cell periphery, and a complete loss of intense, filopodia-based protrusions (Figure 5E, F, G, H, Movie 5). The knockdown phenotype was rescued by re-expression of shRNA resistant RFP-FHOD3 rescue cells, which in fact increased actin polymerisation to form actin spike protrusions and stress fibre-like structures behind the leading edge (Figure 5E, Movie 5). Together, these data indicate that FHOD3 is required for actin polymerisation at the tips of invasive pseudopods downstream of RCP/α5β1 integrin to form filopodia and actin spike-based protrusions that drive invasive migration in 3D ECM.

ROCK-dependent phosphorylation and activation of FHOD3 is required for RCP/α5β1 integrin-driven migration

FHOD3 has no known GTPase interactor/activator, but like FHOD1, can be activated by ROCK-dependent phosphorylation of Ser and Thr residues close to the core DAD motif (Takeya et al., 2008; Iskratsch et al., 2013a). Given that RCP/α5β1 integrin-driven rapid, random migration in 2D is regulated by ROCK (White et al., 2007; Rainero et al., 2012), and that RhoA activity is elevated at the tips of invasive pseudopods in this context (Jacquemet et al., 2013a), we investigated the possibility that ROCK might mediate FHOD3 phosphorylation and activation downstream of RCP/ α5β1 trafficking.

RFP-FHOD3 immunoprecipitated from A2780 cells demonstrated a low level of constitutive Ser/Thr phosphorylation, which was significantly increased upon induction of RCP/ α5β1 trafficking with cRGDfV (Figure 6A). Pre-treatment of cells with a Rho inhibitor, or the highly specific ROCK inhibitor Gly-H1152, opposed cRGDfV-induced FHOD3 phosphorylation (Figure 6A), suggesting that RhoA-ROCK activity promotes FHOD3 phosphorylation. ROCK inhibition also abrogated migration on 3D CDM (Figure 6B, C), and prevented RCP/α5β1 trafficking induced actin spike formation and protrusive area (Figure 6D, E). Interestingly, upon ROCK inhibition protrusions appeared more wavelike, and membrane blebs were not observed (Figure 6D).

Because FHOD3 is phosphorylated by ROCK on 3 conserved residues (Iskratsch et al., 2013a), we mutated each to non-phosphorylatable Ala (3A) or phosphomimetic Asp (3D) within full length shFHOD3#1 resistant RFP-FHOD3 and expressed these in A2780 shFHOD3#1 knockdown cells. Both RFP-FHOD3-3A and –3D showed reduced levels of Ser/Thr phosphorylation compared to wild type RFP-FHOD3 (Figure 7A), and RFP-FHOD3-3A-expressing cells moved more slowly in 3D CDM, whereas expression of RFP-FHOD3-3D

increased migration speed (Figure 7B, C). Furthermore, RFP-FHOD3-3A-expressing cells showed fewer intense F-actin spike protrusions and decreased protrusion size (Figure 7D). Taken together, these data suggest that downstream of RCP/α5β1 trafficking, localised RhoA activity promotes ROCK-dependent phosphorylation and activation of FHOD3 to promote actin polymerisation and filopodia formation at the tips of invasive pseudopods.

FHOD3 is required for RCP/α5β1 integrin-driven invasion *in vitro* and *in vivo*

To assess the role of FHOD3 in invasive migration, we introduced FHOD3 knockdown A2780 or H1299-p53^{273H} cells into inverted invasion assays. FHOD3 knockdown abrogated RCP/α5β1 driven invasion into FN-rich collagen hydrogels (Figure 8A, B, S5D), confirming its requirement in 3D invasive migration. We also injected stable FHOD3 knockdown cells into zebrafish embryos. Whereas control A2780 cells were able to invade into the surrounding stromal environment when RCP/α5β1 recycling was induced, FHOD3 knockdown cells showed little evidence of dissemination (Figure 8C, D). These data suggest that FHOD3 is an actin nucleator that operates downstream of RCP/α5β1 integrin trafficking to promote invasive migration in a physiologically relevant *in vivo* tissue environment.

DISCUSSION

We have shown that lamellipodia formation and retrograde actin flow, which form a major mechanism that drives forward movement of cells in 2D, is observed in cells migrating in 3D matrix. However, promoting RCP/α5β1 trafficking, which increases invasive migration into FN-rich ECM and local invasion *in vivo*, leads to generation of filopodia to form actin spike-based protrusions which extend in the direction of invasion, rather than lamellipodia. Filopodial actin spike protrusions formed in this context require the formin FHOD3, and not Arp2/3-mediated actin polymerisation. This novel form of actin-based protrusion provides the driving force for invasion of cancer cells in 3D ECM *in vitro* and *in vivo*.

In 3D collagen, there is some evidence that lamellipodia can facilitate migration (Giri et al., 2013), and αvβ3 integrin controls lamellipodial migration in 2D (White et al., 2007; Caswell et al., 2008) and promotes invasive migration in low FN microenvironments (Christoforides et al., 2012). Our demonstration of retrograde actin flow in unstimulated cancer cells moving in 3D, within protrusions made up of lamellipodial F-actin veils, provides further evidence to support the notion that the mechanisms that support lamellipodial migration in 2D can facilitate invasive migration in 3D (Figure 1D-F). However, the RCP/α5β1 pathway drives invasion into FN-rich ECM in a manner that does not rely on lamellipodial protrusion, suggesting that alternative mechanisms can drive rapid migration in 3D ECM to contribute to cancer cell invasion and metastasis depending upon the composition of the microenvironment. Loss of the Rac activator Tiam1, or the downstream WAVE complex component CYFIP1, can contribute to cell migration, invasion and metastasis (Malliri et al., 2002; Silva et al., 2009; Vaughan et al., 2014), suggesting that suppression of major regulators of lamellipodia formation can lead to increased metastatic potential.

Non-lamellipodial migratory mechanisms control migration in 3D ECM microenvironments (Friedl and Alexander, 2011; Petrie et al., 2012, 2014), however the RCP/α5β1 pathway promotes migration of cancer cells driven by filopodial actin spike-based protrusions that are morphologically distinct from protrusions seen in amoeboid or lobopodial 3D migration (Figure 1, Figure 2). RCP/α5β1-driven filopodial actin-based protrusions extend beyond the cortex, appear rapidly in collective bursts (Figure 1E-H, S2), show dynamic protrusion and retraction (Figure 1E-H, 2, S2) and the rate of retrograde actin flow is lower than in lamellipodial-based protrusions (Figure 1A-C, Figure S1). Filopodia have been shown to exhibit retrograde F-actin flow (Okabe and Hirokawa, 1991; Lin et al., 1996; Anderson et al., 2008), and interestingly retrograde flow may be reduced in actively protruding filopodia (Mallavarapu and Mitchison, 1999), a notion supported by our data.

Filopodia can arise via at least two broad mechanistic routes: convergent elongation of F-actin derived from the lamellipodial network and tip nucleation through formins (Mattila and Lappalainen, 2008; Mellor, 2010). ArpC3 knockout MEFs retain some ability to migrate in 2D, extending filopodial-like protrusions (FLPs) (Suraneni et al., 2012, 2015), confirming that formins can nucleate actin filaments to generate filopodia in the absence of a dendritic lamellipodial actin network, and here we have shown that filopodia in invasive cells can form in an Arp2/3-independent, FHOD3-driven manner. Long-lived FLPs, formed as a consequence of Rif/mDia2 and integrin signalling, facilitate metastatic colonisation of breast cancer cells (Shibue et al., 2012, 2013). The dynamics of these structures differs from FHOD3-induced filopodia, suggesting that whilst in general integrins may be linked with formin function and filopodial extension, the properties of these filopodial subtypes may be very different. The DRF Rho GTPase effectors have previously been linked to cell migration in 2D and 3D (Kitzing et al., 2010; Vega et al., 2011; Block et al., 2012; Breitsprecher and Goode, 2013). Indeed, we

and others find that members of the formin-like (FMNL) family contribute to basal migration in 3D CDM (Figure 5I; Kitzing et al., 2010; Vega et al., 2011). However, our data suggest that the DRF FHOD3 is specifically required for RCP/α5β1-driven filopodial actin spike formation, migration, and local invasion *in vivo*.

FHOD3 shows relatively restricted expression (heart, kidney and brain; Katoh and Katoh, 2004; Kanaya et al., 2005; Iskratsch et al., 2010), and contributes to sarcomeric organisation in cardiomyocytes by promoting actin polymerisation and contributing to myofibril formation (Taniguchi et al., 2009; Iskratsch et al., 2010). FHOD3 can be activated by ROCK-mediated phosphorylation of Ser/Thr residues within the DAD domain (Iskratsch et al., 2013a), and we now show that FHOD3 is the target of localised RhoA-ROCK signalling downstream of RCP/α5β1 trafficking in invasive cancer cells. However, whilst knockdown of FHOD3 has a profound influence on the morphology of cells in 3D CDM, promoting membrane blebbing (Figure 5E), inhibition of ROCK has a more subtle influence (Figure 6D). ROCK is known to oppose Rac activity through FilGAP (Ohta et al., 2006), and it is therefore possible that ROCK inhibition leads to an increase in Rac activity and formation of lamellipodial protrusions, as observed (Figure 6D). Similarly, expression of non-phosphorylatable FHOD3 induces a more subtle phenotype than knockdown of FHOD3 (Figure 7D). Whilst no RhoGTPase interactor has been described for FHOD3, its closest relative FHOD1 can be activated by Rac binding and/or ROCK phosphorylation, and integrin signalling controls its targeting (Gasteier et al., 2003; Hannemann et al., 2008; Takeya et al., 2008; Iskratsch et al., 2013b). Together with our data this could suggest that numerous signals converge to control the precise local activation of DRFs.

The recycling of α5β1 via the RCP pathway is critical for the establishment of polarised signalling to activate RhoA at the front of migrating and invading cells (Jacquemet et al.,

2013a). WASH is a NPF for Arp2/3 which is required for RCP-mediated α5β1 recycling (Zech et al., 2011), and it is therefore surprising that RCP/α5β1-driven recycling, migration and invasion is unperturbed when Arp2/3 activity is impaired (Figure 3, S3). However, WASH has been reported to interact with the F-actin nucleator Spire (Liu et al., 2009) and V-ATPase (Carnell et al., 2011), which acidifies vesicular compartments, and it is possible that WASH could contribute to α5β1 trafficking in an Arp2/3-independent fashion. The fact that interfering with Arp2/3 function promotes pseudopod extension (Figure 3D, G), accumulation of RCP vesicles at the tips of pseudopods (Figure S3L, M) and is dispensible for α5β1 recycling (Figure S3K) suggests that Arp2/3-mediated actin polymerisation might restrain vesicular cargo, and remodelling of actin (or its disassembly) might be required to facilitate trafficking which leads to downstream signalling to promote migration and invasion.

We have shown that the RCP/α5β1 pathway drives local invasion *in vitro* and *in vivo*, by controlling the activation of FHOD3 to induce filopodial actin spike protrusions in the direction of invasive migration (Figure 3, Figure 7) similar to those seen in FN-rich ECM *in vitro* (Figure 2; Jacquemet et al., 2013a). Breast cancer cell lines expressing GFP-Lifeact implanted into the mammary fat pad of mice in a collagen-rich xenograft environment have been shown to have the ability to generate actin-based protrusions using intravital imaging, but in this context blebbing amoeboid-type migration predominates (Tozluoğlu et al., 2013). In the zebrafish xenograft model, carcinoma cells may migrate in a similar manner to invasive melanoma cells, following collagen I and fibronectin ECM tracks which facilitate invasion (Chapman et al., 2014). This suggests that, as we find *in vitro*, the composition (presence of FN and soluble αvβ3 ligands e.g. osteopontin) and topology of the ECM combine with cell-intrinsic factors (e.g. expression of gain-of-function mutant p53) to produce a migratory response for invasion of stromal environments *in vivo*.

MATERIALS AND METHODS

Cell culture and transient transfection

A2780 cells were cultured in RPMI 1640 (Sigma-Aldrich) supplemented with 10% FCS. H1299, MDA-MB-231, TIF, MEF and 293T cells were cultured in DMEM (Sigma-Aldrich) supplemented with 10% FCS. All cells were maintained at 37°C and 5% CO_2. Transient transfections and siRNA knockdowns were performed using the nucleofector (Solution T; 3 µg plasmid DNA or 1 µM siRNA; program A-23; Amaxa; Lonza), according to the manufacturer's instructions. Formin knockdown was performed with one round of transfection whereas ArpC2 and ArpC3 knockdown was performed with two rounds of transfection.

CDMs were prepared as described previously (Cukierman et al., 2001; Caswell et al., 2008). In brief, plastic tissue-culture plates or glass bottom dishes (for high resolution imaging) were gelatin coated, cross-linked with glutaraldehyde, quenched with glycine, and equilibrated in DMEM containing 10% FCS. Human telomerase-immortalised fibroblasts (TIFs) were seeded at near confluence and grown for 8–10 days in DMEM containing 10% FCS and 50 µg/ml ascorbic acid. Matrices were denuded of live cells by incubation with PBS containing 20 mM NH_4OH and 0.5% Triton X-100, and DNA residue was removed by incubation with DNase I (Lonza).

Plasmids and reagents

Rabbit anti-ArpC2 and ArpC3 antibodies were purchased from Proteintech. Mouse anti-alpha tubulin (DM1A) was purchased from Sigma-Aldrich. Rat anti-RFP antibody and RFP-trap beads were from Chromotek. Rabbit anti-phospho S/T antibody was purchased from ECM biosciences. Affinity purified rabbit anti-FHOD3 was as described (Iskratsch et al., 2010).

DAPI and Alexa-488/555/647 phalloidin were purchased from Life Technologies. Arp2/3 inhibitor CK-666, CK-689 (inactive analogue of CK-666) and ROCK inhibitor Glycyl-H-1152 were purchased from Calbiochem. SMIFH2 was purchased from Sigma-Aldrich. cRGDfV was purchased from BACHEM.

FHOD3 and delta-DAD FHOD3 constructs were as described previously (Iskratsch et al., 2010, 2013a). Photoactivatable (PA) GFP-actin was a gift from K. Anderson. Lifeact-mEGFP and Lifeact-mRFPmars were gifts from R. Wedlich-Soeldner (Riedl et al., 2010), and mTFP1-LifeAct-7 was from AddGene (plasmid #54749).

Knockdown of formins and ArpC2/ArpC3 was performed using siRNA pools from an siARRAY (Dharmacon). Stable FHOD3 shRNA was generated by cloning the following sequences into pLVTHM (Addgene) using Mlu1 and Cla1 restriction sites: FHOD3 shRNA #1 5'-CGCGTCCCC**ATAGACCAGTTGGAGAACAATA**TTCAAGAGA**TATTGTTCTCCAACTGGTCTAT**T-TTTTGGAAAT-3' (adapted from Iskratsch et al., 2010)) and FHOD3 shRNA #2 5'-CGCGTCCCC**ATACGGAGCTACTGGTTTA**TTCAAGAGA**TAAACCAGTAGCTCCGTAT**TTTTTGGAAAT-3'. shRNA resistant FHOD3 was generated using the Q5 Site-directed mutagenesis kit (New England Biolabs) using the following primers: forward 5'-**AGAAAATAAC**AAAACCTTGGGCTT-TATCC-3', reverse 5'- **AATTGATCGAT**TCCTTCCTTCAGGTC-CAG-3'. 3A and 3D mutant RFP-FHOD3 were generated using the following primers: 3A forward 5'- **AAGCTTTGCGAAGAGC-**CCTGAAGAGCGGCCTGAC-3', reverse 5'- **TCCGGTTGGCCCGGGC**TCGTTTCCTCTCCCTCGG-3'. 3D forward 5'- **AAGATTTGCGAAGAGA**CCTGAAGAGCGGCCTGAC-3', reverse 5'- **TCCGG-TTGGCCCGGTC**TCGTTTCCTCTCCCTCGG-3'. Lifeact-mRFPmars was subcloned into pCDH (gift from A. Gilmore) using restriction sites EcoRI and NotI, and shRNA resistant RFP-FHOD3 was cloned into pCDH using Nhe1 and Not1.

Lentiviral production and transduction

Lentiviruses were produced by transfecting 293T cells with psPAX2 and pMD2.G (Addgene) and pLVTHM or pCDH viral vectors. Conditioned medium containing viruses was collected after 5 days and then used immediately to infect cells or stored at −80°C. Infected cells were sorted for EGFP or mRFPMars expression using FACS ARIA Fusion (BD Biosciences) with excitation at 488nm and 561nm respectively. FACS data was processed and analysed using DIVA8 software (BD Biosciences).

SDS-PAGE and quantitative Western blotting

Cells were lysed in lysis buffer (200 mM NaCl, 75 mM Tris-HCl, pH 7.4, 15 mM NaF, 1.5 mM Na_3VO_4, 7.5 mM EDTA, 7.5 mM EGTA, 1.5% (v/v) Triton X-100, 0.75% (v/v) NP-40, 50 µg/ml leupeptin, 50 µg/ml aprotinin, and 1 mM 4-(2-aminoethyl)-benzenesulfonyl fluoride). Lysates were clarified by centrifugation at 10,000 g for 10 min at 4°C.

Cell lysates were resolved under denaturing conditions by SDS-PAGE (4–12% Bis-Tris gels; Invitrogen) and transferred to nitrocellulose membrane. Membranes were blocked and incubated overnight at 4°C with the appropriate primary antibody and then at room temperature for 1 h with the appropriate fluorophore-conjugated secondary antibody. Membranes were scanned using an infrared imaging system (Odyssey; LI-COR Biosciences). Band intensity was determined by digital densitometric analysis using Image Studio (version 4.0). Western blots shown are representative of at least three independent experiments.

RNA extraction and PCRs

RNA was extracted from cells using TRI Reagent (Sigma-Aldrich) according to the manufacturer's instructions.

For real-time qPCR, reactions were performed using the Power SYBR Green RNA-to-CT 1-Step Kit (Applied Biosystems) with 1µg RNA template and run using a StepOnePlus Real-Time PCR System and StepOnePlus software (Applied Biosystems). Fold change in gene expression was calculated using the comparative CT method (Schmittgen and Livak, 2008). Primers used in the reactions are listed in Supplemental Table 2 in (Kitzing et al., 2010). GAPDH expression was used as an endogenous control.

For reverse transcription PCR, reactions were performed using the OneStep RT-PCR Kit (QIAGEN) with 1µg RNA template and either pan-FHOD3 forward primer 5'-CTCCTTTTTACTCTTTATGGGCCATCC-3' or muscle-specific FHOD3 forward primer 5'-ACTGATGAGGAGGAGGAAGTTGAG-3' with pan-FHOD3 reverse primer 5'-CTCGCTGACTGGGCACTTGGGTGG-3'.

Microscopy

All images were taken with a constant exposure time between all the conditions of the same experiment. Images were processed using Image J v1.49b (NIH) and only subjected to signal re-scaling using linear transformation for display in the figures.

For 2D scratch wound assays, cells were seeded onto tissue culture plates to confluency and after 24 hours cell monolayers were wounded with a plastic pipette tip. For 3D migration assays, cells were plated onto CDM for >4 hours. For long-term time lapse, cells were imaged in the presence or absence of cRGDfV and maintained at 37°C and 5% CO_2. Phase-contrast images were captured on an inverted microscope system (AS-MDW; Leica) using a 20× objective (HC Plan Fluotar Ph2, NA 0.50) every 10 min using a charge-coupled device (CCD) camera (CoolSNAP HQ; Photometrics) and the Micro-Manager plugin for ImageJ (version 1.4.17; Edelstein et al., 2010, 2014). Point visiting mode was used to allow multiple

positions to be imaged within the same timecourse. Images and videos were analysed using ImageJ with the MTrackJ plugin (Meijering et al., 2012). Analysis of speed, endpoint directional persistence, direction autocorrelation and mean square displacement (MSD) was performed using DiPer (Gorelik and Gautreau, 2014). Endpoint directional persistence and autocorrelation (a measure of directionality less influenced by speed) were used in 2D to accurately reflect a cell's ability to migrate in a persistent manner, but this is less appropriate in 3D CDM where cells generally follow the fibrillar nature of the ECM. We therefore used MSD (a measure of the area explored) to better define migration capacity in 3D CDM. To obtain a measure of pseudopod length, the distance between the centre of the nucleus and the cell front (with respect to the direction of migration) was measured using ImageJ.

Wounded cells fixed with 4% paraformaldehyde were stained with FITC-phalloidin and DAPI and imaged with a Delta Vision RT (Applied Precision) restoration microscope using a 40x/NA 1.30 Uplan FLN objective and Sedat filter set (86000v2; Chroma). Images were collected using a Coolsnap HQ camera (Photometrics).

For photoactivation, cells transiently co-transfected with Lifeact-mRFPmars and paGFP-Actin were seeded onto glass-bottom dishes or CDMs and media replaced by Ham's F12 (Gibco) containing 25 mM HEPES and 10% FCS before addition of cRGDfV (>2 hours) where appropriate for image acquisition. Using a spinning disk confocal inverted microscope (Marianas, 3i). paGFP-Actin was photoactivated at cell protrusions within a square region of interest (ROI; $5um^2$) for 10ms using a 405nm laser. paGFP and mRFPMars fluorescence emission was captured every second for 100s using a 63x objective (NA 1.4 Plan Apochromat) and SlideBook 6.0 software. Images analysis was performed in ImageJ: ROIs were positioned over the point of photoactivation, immediately behind the photactivated region (relative to the direction of protrusion) or outside the area of the cell (used for background subtraction).

Fluorescence intensity was normalised to the intensity of the photoactivated region in the first frame after photoactivation.

For live-cell imaging of actin dynamics during invasive migration, A2780, H1299 and MDA-MB-231 cells transiently transfected with Lifeact-mEGFP or Lifeact-mTFP1 were plated on CDMs for 4 h and normal culture medium was replaced by Ham's F12 containing 25 mM HEPES and 10% FCS before addition of cRGDfV (>2 hours) where appropriate before image acquisition. Image stacks (7 positions every 0.2µm) were collected every 1 min (Lifeact-mEGFP) or 3 min (Lifeact-mTFP1) at 37°C on a spinning disk confocal inverted microscope (Marianas) using a 63× objective (NA 1.4 Plan Apochromat) and SlideBook 6.0 software.

RFP- or RFP-FHOD3-expressing cells were seeded onto CDMs 4 hours prior to treatment with cRGDfV for 2 hours as appropriate. Cells were fixed with 4% paraformaldehyde and stained with rat anti-RFP primary antibody (ChromoTek), Rhodamine Red-X-conjugated secondary antibody (Jackson ImmunoResearch) and Alexa Fluor 647-phalloidin (Life Technologies). Cells were imaged with a Delta Vision RT (Applied Precision) restoration microscope using a 60x/NA 1.42 Plan Apo objective and the Sedat filter set (86000v2, Chroma). Images were collected using a Coolsnap HQ (Photometrics) camera with a Z optical spacing of 0.2µm. Raw images were then deconvolved (aggressive mode, 10 pass) using SoftWorx software (Applied Precision) and maximum intensity projections of these deconvolved images are shown.

Structured illumination microscopy was performed on Alexa-488 Phalloidin stained A2780 cells on CDM. Images were acquired on a Zeiss ELYRA S.1 system with a pco.edge 5.5 scientific CMOS camera using a 63x/1.4 NA oil immersion objective lens. For optimal lateral spatial sampling a 1.6x intermediate magnification lens was used, resulting in a pixel size of 64 nm. A z-interval of 110 nm was used to ensure adequate spatial sampling in the axial

dimension. Excitation was achieved with a 488 nm laser and emission was filtered with a 495-550 nm band pass filter. Modulation of the illumination light was achieved using a physical grating with 28 µm spacing. For each z plane this patterned illumination was shifted through 5 phases at each of 5 rotational angles. Raw data were processed using ZEN software and analysed using ImageJ and the Matlab application CellGeo (Tsygankov et al., 2014) to determine filopodia number and length, respectively.

Quantification of actin protrusions in 3D CDM was performed using maximum Z projections of cells imaged for 30-60 mins. Using custom software written in Python and NumPy, images in the timelapse sequence were individually band-pass filtered (A trous wavelet, linear 3x3 filter, keeping scales 2-8) to remove both high frequency noise and stationary background. Images were thresholded using a fixed threshold (pixel grey value above 100) and all the objects in the resulting binary image were identified using an 8-connected component labelling. All but the largest object in the image were discarded. The difference between binary images with a lag of 3 mins between frames was used to identify protrusive areas. In order to limit the analysis to the front of the cell only, the following automated method was devised: the axis aligned minimum bounding box was calculated for each cell at each time point, and divided into three equal parts along the longer axis. The area of protrusions was normalised to the total area of the cell and protrusive areas within the front region were used to generate shape description measurements. Mean values were generated from >25 frames per cell.

Zebrafish xenograft assay

Zebrafish (*Danio rerio*) were maintained at the University of Manchester Biological Services Unit according to National Home Office regulations under the Animals (Scientific

Procedures) Act 1986. *Casper* strain (*roy*-/-, *nacre*-/-) zebrafish were used throughout the study to generate embryos completely lacking pigment which can otherwise obscure imaging. H1299 cells, A2780 cells, or A2780 cells stably expressing Lifeact-mRFPmars, pLVTHM vector control or shFHOD3 were stained with carboxyfluorescein succinimidyl ester (CFSE, Life Technologies) 24 hours prior to injection. Suspended cells were injected into the pericardial cavity of 48 hour postfertilisation zebrafish embryos. cRGDfV was added, where appropriate, 1 day post injection (dpi). Prior to imaging zebrafish were mounted in 1.5 % low melting agarose (LMP, Flowgen Biosciences). Lifeact-mRFPmars-expressing cells were imaged 3dpi using a spinning disk confocal inverted microscope using a long working distance 63x objective (NA 1.15, C Apochromat). Z-stacks were rendered using Imaris (version 8.0). Wild type, vector control and shFHOD3 4 dpi engrafted tumours were imaged using a Leica TCS SP5 AOBS upright confocal (Leica Microsystems) using a 20x 0.50 Plan Fluotar dipping objective and 1.5x confocal zoom. Relative invasion was defined as the mean number of cells located outside the pericardial cavity at 4dpi normalised to the average number of cells in the control condition.

Inverted invasion assays

Inverted invasion assays were modified from those described previously (Hennigan et al., 1994). In brief, collagen I (final concentration ~5 μg/ml; BD Biosciences) supplemented with 25 μg/ml FN was allowed to polymerise in inserts (Transwell; Corning) for 1 h at 37°C. Inserts were then inverted, and cells were seeded directly onto the opposite face of the filter. Transwell inserts were finally placed in 0.1% serum medium, and medium supplemented with 10% FCS and 30 ng/ml EGF was placed on top of the matrix, providing a chemotactic gradient. Where appropriate, cRGDfV was added to the matrix before plug polymerisation and also to

the medium throughout the system. 48–72 h after seeding, migrating cells were stained with Calcein-AM and visualised by confocal microscopy with serial optical sections being captured at 15-µm intervals using an inverted confocal microscope (TCS SP5 AOBS; Leica) using a 20× objective. Invasion was quantified using the area calculator plugin in ImageJ, measuring the fluorescence intensity of cells invading 45 µm or more and expressing this as a percentage of the fluorescence intensity of all cells within the plug.

Integrin Recycling Assay

Recycling assays were performed as described previously (Caswell et al., 2008). Receptor internalization conditions were 30 min at 37°C in serum free medium. The antibodies used for capture ELISA detection of α5β1 integrin were obtained from BD Biosciences. cRGDfV, CK-689 and CK-666 were added to the cells only during the recycling period.

Statistical analysis

Student's *t*-test (unpaired, two tailed, and unequal variance) or ANOVA/Tukey's multiple comparison test were used to calculate statistical significance as appropriate, using GraphPad Prism version 6 (GraphPad Software). $t_{1/2}$ (Figure 1, S1) was approximated using non-linear regression (exponential one-phase decay; GraphPad Prism). Bar charts (+/-SEM) or Tukey box and whisker plots are displayed (whiskers represent 1.5x interquartile range, + indicates mean).

Online supplemental material

Figure S1 show retrograde flow in A2780 and H1299 cells in 2D and MDA-MB-231 cells in 3D CDM. Figure S2 shows the dynamics of Lifeact-GFP in H1299 and MDA-MB-231 cells, and

filopodial lifetime of A2780 cells in 3D CDM. Figure S3 shows the effect of Arp2/3 inhibition/knockdown on migration in 2D and 3D, and the effect of Arp2/3 inhibition on integrin recycling and vesicle localisation. Figure S4 show formin knockdown by qPCR, the effect of FHOD3 knockdown on 2D migration and confirms that cancer cells do not express FHOD3 with the muscle specific exon 26. Figure S5 shows the localisation of RFP-FHOD3wt and an active FHOD3, and knockdown of FHOD3 in H1299-273H cells. Movie 1 shows retrograde flow of actin in A2780 cells on CDM, movie 2 shows the dynamics of Lifeact-GFP in A2780 cells on CDM. Movie 3 demonstrates that A2780 cells form filopodial actin spikes as they invade *in vivo*, and Movie 4 shows the effect of Arp2/3 inhibition on Lifeact-GFP dynamics in A2780 cells on CDM. Movies 5,6 and 7 shows the effect of FHOD3 knockdown and rescue and ROCK inhibition on Lifeact-GFP dynamics in A2780 cells on CDM.

Acknowledgements

We thank the Bioimaging Facility for their help with microscopy; microscopes used in this study were purchased with grants from BBSRC, the Wellcome Trust and the University of Manchester Strategic Fund. We thank M. Jackson and G. Howell for assistance with FACS, and David Bradley for technical support. We thank Robert Grosse for providing advice and reagents for formin knockdown, and Roman Gorelik for assistance with DiPer. The work of our laboratories is supported by the Wellcome Trust (090453/Z/09/Z and 090453/Z/09/A, PTC), Worldwide Cancer Research (14- 1226, PTC), European Research Council (ERC-2011-StG-282059, AH) and The Dowager Countess Eleanor Peel Trust (TH-PRCL.FID2228, AH). The Wellcome Trust Centre for Cell-Matrix Research is supported by grant 088785/Z/09/Z.

REFERENCES

Adorno, M., M. Cordenonsi, M. Montagner, S. Dupont, C. Wong, B. Hann, A. Solari, S. Bobisse, M.B. Rondina, V. Guzzardo, A.R. Parenti, A. Rosato, S. Bicciato, A. Balmain, and S. Piccolo. 2009. A Mutant-p53/Smad Complex Opposes p63 to Empower TGFbeta-Induced Metastasis. *Cell*. 137:87–98. doi:10.1016/j.cell.2009.01.039.

Anderson, T.W., A.N. Vaughan, and L.P. Cramer. 2008. Retrograde Flow and Myosin II Activity within the Leading Cell Edge Deliver F-Actin to the Lamella to Seed the Formation of Graded Polarity Actomyosin II Filament Bundles in Migrating Fibroblasts Tom. *Mol. Biol. Cell*. 19:5006–5018. doi:10.1091/mbc.E08.

Arjonen, A., R. Kaukonen, E. Mattila, P. Rouhi, G. Hognas, H. Sihto, B.W. Miller, J.P. Morton, E. Bucher, P. Taimen, R. Virtakoivu, Y. Cao, O.J. Sansom, H. Joensuu, and J. Ivaska. 2014. Mutant p53-associated myosin-X upregulation promotes breast cancer invasion and metastasis. *J. Clin. Invest.* 124:1069–1082. doi:10.1172/JCI67280DS1.

Block, J., D. Breitsprecher, S. Kühn, M. Winterhoff, F. Kage, R. Geffers, P. Duwe, J.L. Rohn, B. Baum, C. Brakebusch, M. Geyer, T.E.B. Stradal, J. Faix, and K. Rottner. 2012. FMNL2 drives actin-based protrusion and migration downstream of Cdc42. *Curr. Biol.* 22:1005–1012. doi:10.1016/j.cub.2012.03.064.

Bravo-Cordero, J.J., L. Hodgson, and J. Condeelis. 2012. Directed cell invasion and migration during metastasis. *Curr. Opin. Cell Biol.* 24:277–83. doi:10.1016/j.ceb.2011.12.004.

Breitsprecher, D., and B.L. Goode. 2013. Formins at a glance. *J. Cell Sci.* 126:1–7. doi:10.1242/jcs.107250.

Bridgewater, R.E., J.C. Norman, and P.T. Caswell. 2012. Integrin trafficking at a glance. *J. Cell Sci.* 125:3695–3701.

Carnell, M., T. Zech, S.D. Calaminus, S. Ura, M. Hagedorn, S.A. Johnston, R.C. May, T. Soldati, L.M. Machesky, and R.H. Insall. 2011. Actin polymerization driven by WASH causes V-ATPase retrieval and vesicle neutralization before exocytosis. *J. Cell Biol.* 193:831–839. doi:10.1083/jcb.201009119.

Caswell, P.T., M. Chan, A.J. Lindsay, M.W. McCaffrey, D. Boettiger, and J.C. Norman. 2008. Rab-coupling protein coordinates recycling of alpha5beta1 integrin and EGFR1 to promote cell migration in 3D microenvironments. *J. Cell Biol.* 183:143–55. doi:10.1083/jcb.200804140.

Caswell, P.T., and J. Norman. 2008. Endocytic transport of integrins during cell migration and invasion. *Trends Cell Biol.* 18:257–63. doi:10.1016/j.tcb.2008.03.004.

Caswell, P.T., and J.C. Norman. 2006. Integrin trafficking and the control of cell migration. *Traffic*. 7:14–21. doi:10.1111/j.1600-0854.2005.00362.x.

Caswell, P.T., H.J. Spence, M. Parsons, D.P. White, K. Clark, K.W. Cheng, G.B. Mills, M.J. Humphries, A.J. Messent, K.I. Anderson, M.W. McCaffrey, B.W. Ozanne, and J.C. Norman. 2007. Rab25 associates with alpha5beta1 integrin to promote invasive migration in 3D microenvironments. *Dev. Cell*. 13:496–510. doi:10.1016/j.devcel.2007.08.012.

Caswell, P.T., S. Vadrevu, and J.C. Norman. 2009. Integrins: masters and slaves of endocytic transport. *Nat. Rev. Mol. Cell Biol.* 10:843–53. doi:10.1038/nrm2799.

Caulin, C., T. Nguyen, G.A. Lang, T.M. Goepfert, B.R. Brinkley, W. Cai, G. Lozano, and D.R. Roop. 2007. An inducible mouse model for skin cancer reveals distinct roles for gain- and loss-of-function p53 mutations. *J. Clin. Invest.* 117:1893–1901. doi:10.1172/JCI31721.result.

Chapman, A., L. Fernandez del Ama, J. Ferguson, J. Kamarashev, C. Wellbrock, and A. Hurlstone. 2014. Heterogeneous tumor subpopulations cooperate to drive invasion. *Cell Rep.* 8:688–95. doi:10.1016/j.celrep.2014.06.045.

Christoforides, C., E. Rainero, K.K. Brown, J.C. Norman, and A. Toker. 2012. PKD controls αvβ3 integrin recycling and tumor cell invasive migration through its substrate Rabaptin-5. *Dev. Cell*. 23:560–72. doi:10.1016/j.devcel.2012.08.008.

Cukierman, E., R. Pankov, D.R. Stevens, and K.M. Yamada. 2001. Taking cell-matrix adhesions to the third dimension. *Science*. 294:1708–12. doi:10.1126/science.1064829.

Desgrosellier, J.S., and D.A. Cheresh. 2010. Integrins in cancer: biological implications and therapeutic opportunities. *Nat. Rev. Cancer*. 10:9–22. doi:10.1038/nrc2748.

Doyle, B., J.P. Morton, D.W. Delaney, R.A. Ridgway, J.A. Wilkins, and O.J. Sansom. 2010. p53 mutation and loss have different effects on tumourigenesis in a novel mouse model of pleomorphic rhabdomyosarcoma. *J. Pathol.* 129–137.

Dozynkiewicz, M.A., N.B. Jamieson, I. Macpherson, J. Grindlay, P.V.E. van den Berghe, A. von Thun, J.P. Morton, C. Gourley, P. Timpson, C. Nixon, C.J. McKay, R. Carter, D. Strachan, K. Anderson, O.J. Sansom, P.T. Caswell, and J.C. Norman. 2012. Rab25 and CLIC3 collaborate to promote integrin recycling from late endosomes/lysosomes and drive cancer progression. *Dev. Cell*. 22:131–45. doi:10.1016/j.devcel.2011.11.008.

Edelstein, A., N. Amodaj, K. Hoover, R. Vale, and N. Stuurman. 2010. Computer control of microscopes using manager. 14.20. 1-17 pp.

Edelstein, A.D., M.A. Tsuchida, N. Amodaj, H. Pinkard, R.D. Vale, and N. Stuurman. 2014. Advanced methods of microscope control using μ Manager software. *J. Biol. Methods*. 1:1–10. doi:10.14440/jbm.2014.36.

Friedl, P., and S. Alexander. 2011. Cancer Invasion and the Microenvironment: Plasticity and Reciprocity. *Cell*. 147:992–1009. doi:10.1016/j.cell.2011.11.016.

Friedl, P., J. Locker, E. Sahai, and J.E. Segall. 2012. Classifying collective cancer cell invasion. *Nat. Cell Biol.* 14:777–83. doi:10.1038/ncb2548.

Gardel, M.L., B. Sabass, L. Ji, G. Danuser, U.S. Schwarz, and C.M. Waterman. 2008. Traction stress in focal adhesions correlates biphasically with actin retrograde fl ow speed. *J. Cell Biol.* 183:999–1005. doi:10.1083/jcb.200810060.

Gasteier, J.E., R. Madrid, E. Krautkrämer, S. Schröder, W. Muranyi, S. Benichou, and O.T. Fackler. 2003. Activation of the Rac-binding partner FHOD1 induces actin stress fibers via a ROCK-dependent mechanism. *J. Biol. Chem.* 278:38902–38912. doi:10.1074/jbc.M306229200.

Giri, A., S. Bajpai, N. Trenton, H. Jayatilaka, G.D. Longmore, and D. Wirtz. 2013. The Arp2/3 complex mediates multigeneration dendritic protrusions for efficient 3-dimensional cancer cell migration. *FASEB J.* 27:4089–4099. doi:10.1096/fj.12-224352.

Gorelik, R., and A. Gautreau. 2014. Quantitative and unbiased analysis of directional persistence in cell migration. *Nat. Protoc.* 9:1931–1943. doi:10.1038/nprot.2014.131.

Hannemann, S., R. Madrid, J. Stastna, T. Kitzing, J. Gasteier, A. Schönichen, J. Bouchet, A. Jimenez, M. Geyer, R. Grosse, S. Benichou, and O.T. Fackler. 2008. The diaphanous-related formin FHOD1 associates with ROCK1 and promotes Src-dependent plasma membrane blebbing. *J. Biol. Chem.* 283:27891–27903. doi:10.1074/jbc.M801800200.

Hennigan, R.F., K.L. Hawker, and B.W. Ozanne. 1994. Fos-transformation activates genes associated with invasion. *Oncogene*. 9:3591–600.

Hynes, R.O. 2002. Integrins : Bidirectional , Allosteric Signaling Machines. *Cell*. 110:673–687.

Iskratsch, T., S. Lange, J. Dwyer, A.L. Kho, C. dos Remedios, and E. Ehler. 2010. Formin follows function: a muscle-specific isoform of FHOD3 is regulated by CK2 phosphorylation and promotes myofibril maintenance. *J. Cell Biol.* 191:1159–72. doi:10.1083/jcb.201005060.

Iskratsch, T., S. Reijntjes, J. Dwyer, P. Toselli, I.R. Dégano, I. Dominguez, and E. Ehler. 2013a. Two distinct phosphorylation events govern the function of muscle FHOD3. *Cell. Mol. Life Sci.* 70:893–908. doi:10.1007/s00018-012-1154-7.

Iskratsch, T., C.-H. Yu, A. Mathur, S. Liu, V. Stévenin, J. Dwyer, J. Hone, E. Ehler, and M. Sheetz. 2013b. FHOD1 Is Needed for Directed Forces and Adhesion Maturation during Cell Spreading and Migration. *Dev. Cell*. 27:545–59. doi:10.1016/j.devcel.2013.11.003.

Ivaska, J., and J. Heino. 2011. Cooperation between integrins and growth factor receptors in signaling and endocytosis. *Annu. Rev. Cell Dev. Biol.* 27:291–320. doi:10.1146/annurev-cellbio-092910-154017.

Jacquemet, G., D.M. Green, R.E. Bridgewater, A. von Kriegsheim, M.J. Humphries, J.C. Norman, and P.T. Caswell. 2013a. RCP-driven α5β1 recycling suppresses Rac and

promotes RhoA activity via the RacGAP1-IQGAP1 complex. *J. Cell Biol.* 202:917–35. doi:10.1083/jcb.201302041.

Jacquemet, G., M.J. Humphries, and P.T. Caswell. 2013b. Role of adhesion receptor trafficking in 3D cell migration. *Curr. Opin. Cell Biol.* 25:627–32. doi:10.1016/j.ceb.2013.05.008.

Kanaya, H., R. Takeya, K. Takeuchi, N. Watanabe, N. Jing, and H. Sumimoto. 2005. Fhos2, a novel formin-related actin-organizing protein, probably associates with the nestin intermediate filament. *Genes to Cells*. 10:665–678. doi:10.1111/j.1365-2443.2005.00867.x.

Katoh, M., and M. Katoh. 2004. Identification and characterization of human FHOD3 gene in silico. *Int. J. Mol. Med.* 13:615–620.

Kaur, S., H.A. Kenny, S. Jagadeeswaran, M.R. Zillhardt, A.G. Montag, E. Kistner, S.D. Yamada, A.K. Mitra, and E. Lengyel. 2009. {Beta}3-Integrin Expression on Tumor Cells Inhibits Tumor Progression, Reduces Metastasis, and Is Associated With a Favorable Prognosis in Patients With Ovarian Cancer. *Am. J. Pathol.* 175:2184–96. doi:10.2353/ajpath.2009.090028.

Kitzing, T.M., Y. Wang, O. Pertz, J.W. Copeland, and R. Grosse. 2010. Formin-like 2 drives amoeboid invasive cell motility downstream of RhoC. *Oncogene*. 29:2441–8. doi:10.1038/onc.2009.515.

Krause, M., and A. Gautreau. 2014. Steering cell migration: lamellipodium dynamics and the regulation of directional persistence. *Nat. Rev. Mol. Cell Biol.* 15:577–590. doi:10.1038/nrm3861.

Lai, F.P., M. Szczodrak, J. Block, J. Faix, H.G. Mannherz, T.E.B. Stradal, G.A. Dunn, J.V. Small, and K. Rottner. 2008. Arp2/3 complex interactions and actin network turnover in lamellipodia. *EMBO J.* 27:982–992. doi:10.1038/emboj.2008.34.

Law, A.-L., A. Vehlow, M. Kotini, L. Dodgson, D. Soong, E. Theveneau, C. Bodo, E. Taylor, C. Navarro, U. Perera, M. Michael, G.A. Dunn, D. Bennett, R. Mayor, and M. Krause. 2013. Lamellipodin and the Scar/WAVE complex cooperate to promote cell migration in vivo. *J. Cell Biol.* 203:673–89. doi:10.1083/jcb.201304051.

Legate, K.R., S.A. Wickström, and R. Fässler. 2009. Genetic and cell biological analysis of integrin outside-in signaling. *Genes Dev.* 23:397–418. doi:10.1101/gad.1758709.

Lin, C.H., E.M. Espreafico, M.S. Mooseker, and P. Forscher. 1996. Myosin drives retrograde F-actin flow in neuronal growth cones. *Neuron*. 16:769–782. doi:10.1016/S0896-6273(00)80097-5.

Liu, R., M.T. Abreu-Blanco, K.C. Barry, E. V Linardopoulou, G.E. Osborn, and S.M. Parkhurst. 2009. Wash functions downstream of Rho and links linear and branched actin nucleation factors. *Development*. 136:2849–60. doi:10.1242/dev.035246.

Mallavarapu, A., and T. Mitchison. 1999. Regulated actin cytoskeleton assembly at filopodium tips controls their extension and retraction. *J. Cell Biol.* 146:1097–1106. doi:10.1083/jcb.146.5.1097.

Malliri, A., R.A. van der Kammen, K. Clark, M. van der Valk, F. Michiels, and J.G. Collard. 2002. Mice deficient in the Rac activator Tiam1 are resistant to Ras-induced skin tumours. *Nature*. 417:867–871. doi:10.1038/nature00848.

Mattila, P.K., and P. Lappalainen. 2008. Filopodia: molecular architecture and cellular functions. *Nat. Rev. Mol. Cell Biol.* 9:446–54. doi:10.1038/nrm2406.

Maubant, S., S. Cruet-Hennequart, S. Dutoit, Y. Denoux, H. Crouet, M. Henry-Amar, and P. Gauduchon. 2005. Expression of α V-associated integrin β subunits in epithelial ovarian cancer andits relation to prognosis in patients treated with platinum-based regimens. *J. Mol. Histol.* 36:119–129. doi:10.1007/s10735-004-4273-0.

Meijering, E., O. Dzyubachyk, and I. Smal. 2012. Methods for cell and particle tracking. *Methods Enzymol.* 504:183–200.

Mellor, H. 2010. The role of formins in filopodia formation. *Biochim. Biophys. Acta*. 1803:191–200. doi:10.1016/j.bbamcr.2008.12.018.

Muller, P.A.J., P.T. Caswell, B. Doyle, M.P. Iwanicki, E.H. Tan, S. Karim, N. Lukashchuk, D.A. Gillespie, R.L. Ludwig, P. Gosselin, A. Cromer, J.S. Brugge, O.J. Sansom, J.C. Norman, and K.H. Vousden. 2009. Mutant p53 drives invasion by promoting integrin recycling. *Cell*. 139:1327–41. doi:10.1016/j.cell.2009.11.026.

Muller, P.A.J., A.G. Trinidad, P. Timpson, J.P. Morton, S. Zanivan, P.V.E. van den Berghe, C. Nixon, S. a Karim, P.T. Caswell, J.E. Noll, C.R. Coffill, D.P. Lane, O.J. Sansom, P.M. Neilsen, J.C. Norman, and K.H. Vousden. 2013. Mutant p53 enhances MET trafficking and signalling to drive cell scattering and invasion. *Oncogene*. 32:1252–65. doi:10.1038/onc.2012.148.

Nolen, B.J., N. Tomasevic, A. Russell, D.W. Pierce, Z. Jia, C.D. McCormick, J. Hartman, R. Sakowicz, and T.D. Pollard. 2009. Characterization of two classes of small molecule inhibitors of Arp2/3 complex. *Nature*. 460:1031–1034. doi:10.1038/nature08231.

Nürnberg, A., T. Kitzing, and R. Grosse. 2011. Nucleating actin for invasion. *Nat. Rev. cancer*. 11:177–187. doi:10.1038/nrc3003.

Ohta, Y., J.H. Hartwig, and T.P. Stossel. 2006. FilGAP, a Rho- and ROCK-regulated GAP for Rac binds filamin A to control actin remodelling. *Nat. Cell Biol.* 8:803–814. doi:10.1038/ncb1437.

Okabe, S., and N. Hirokawa. 1991. Actin dynamics in growth cones. *J. Neurosci.* 11:1918–1929.

Pellegrin, S., and H. Mellor. 2005. The Rho Family GTPase Rif Induces Filopodia through mDia2. *Curr. Biol.* 15:129–133. doi:10.1016/j.

Pellinen, T., and J. Ivaska. 2006. Integrin traffic. *J. Cell Sci.* 119:3723–31. doi:10.1242/jcs.03216.

Peng, J., B.J. Wallar, A. Flanders, P.J. Swiatek, and A.S. Alberts. 2003. Disruption of the Diaphanous-Related Formin Drf1 Gene Encoding mDia1 Reveals a Role for Drf3 as an Effector for Cdc42. *Curr. Biol.* 13:534–545. doi:10.1016/S.

Petrie, R.J., N. Gavara, R.S. Chadwick, and K.M. Yamada. 2012. Nonpolarized signaling reveals two distinct modes of 3D cell migration. *J. Cell Biol.* 197:439–455.

Petrie, R.J., H. Koo, and K.M. Yamada. 2014. Generation of compartmentalized pressure by a nuclear piston governs cell motility in a 3D matrix. *Science*. 345:1062–5. doi:10.1126/science.1256965.

Rainero, E., P.T. Caswell, P.A.J. Muller, J. Grindlay, W. Mary, Q. Zhang, M.J.O. Wakelam, K.H. Vousden, A. Graziani, and J.C. Norman. 2012. Diacylglycerol kinase-α controls RCP-dependent integrin trafficking to promote invasive migration. *J. Cell Biol.* 196:277–295.

Riedl, J., A.H. Crevenna, K. Kessenbrock, J.H. Yu, M. Bista, F. Bradke, D. Jenne, T.A. Holak, Z. Werb, M. Sixt, and R. Wedlich-Soldner. 2010. Lifeact: a versatile marker to visualize F-actin. *Nat. Methods*. 5:605–607. doi:10.1038/nmeth.1220.Lifeact.

Rizvi, S.A., E.M. Neidt, J. Cui, Z. Feiger, C.T. Skau, M.L. Gardel, S.A. Kozmin, and D.R. Kovar. 2009. Identification and Characterization of a Small Molecule Inhibitor of Formin-Mediated Actin Assembly. *Chem. Biol.* 16:1158–1168. doi:10.1016/j.chembiol.2009.10.006.

Sanz-Moreno, V., G. Gadea, J. Ahn, H. Paterson, P. Marra, S. Pinner, E. Sahai, and C.J. Marshall. 2008. Rac activation and inactivation control plasticity of tumor cell movement. *Cell*. 135:510–23. doi:10.1016/j.cell.2008.09.043.

Sawada, K., A.K.K. Mitra, a R.R. Radjabi, V. Bhaskar, E.O.O. Kistner, M. Tretiakova, S. Jagadeeswaran, A. Montag, A. Becker, H. a a Kenny, M.E.E. Peter, V. Ramakrishnan, S.D.D. Yamada, and E. Lengyel. 2008. Loss of E-cadherin promotes ovarian cancer metastasis via alpha 5-integrin, which is a therapeutic target. *Cancer Res.* 68:2329–39. doi:10.1158/0008-5472.CAN-07-5167.

Shibue, T., M.W. Brooks, M.F. Inan, F. Reinhardt, and R.A. Weinberg. 2012. The outgrowth of micrometastases is enabled by the formation of filopodium-like protrusions. *Cancer Discov.* 2:706–721.

Shibue, T., M.W. Brooks, and R.A. Weinberg. 2013. An Integrin-Linked Machinery of Cytoskeletal Regulation that Enables Experimental Tumor Initiation and Metastatic Colonization. *Cancer Cell*. 24:481–498. doi:10.1016/j.ccr.2013.08.012.

Silva, J.M., E. Ezhkova, J. Silva, S. Heart, M. Castillo, Y. Campos, V. Castro, F. Bonilla, C. Cordon-Cardo, S.K. Muthuswamy, S. Powers, E. Fuchs, and G.J. Hannon. 2009. Cyfip1 is a putative

invasion suppressor in epithelial cancers. *Cell*. 137:1047–1061. doi:10.1016/j.cell.2009.04.013.Cyfip1.

Suraneni, P., B. Fogelson, B. Rubinstein, P. Noguera, N. Volkmann, D. Hanein, A. Mogilner, and R. Li. 2015. A Mechanism of Leading Edge Protrusion in the Absence of Arp2/3 Complex. *Mol. Biol. Cell*. 26. doi:10.1091/mbc.E14-07-1250.

Suraneni, P., B. Rubinstein, J.R. Unruh, M. Durnin, D. Hanein, and R. Li. 2012. The Arp2/3 complex is required for lamellipodia extension and directional fibroblast cell migration. *J. Cell Biol.* 197:239–251. doi:10.1083/jcb.201112113.

Takeya, R., K. Taniguchi, S. Narumiya, and H. Sumimoto. 2008. The mammalian formin FHOD1 is activated through phosphorylation by ROCK and mediates thrombin-induced stress fibre formation in endothelial cells. *EMBO J.* 27:618–628. doi:10.1038/emboj.2008.7.

Taniguchi, K., R. Takeya, S. Suetsugu, M. Kan-o, M. Narusawa, A. Shiose, R. Tominaga, and H. Sumimoto. 2009. Mammalian formin Fhod3 regulates actin assembly and sarcomere organization in striated muscles. *J. Biol. Chem.* 284:29873–29881. doi:10.1074/jbc.M109.059303.

Theveneau, E., and R. Mayor. 2013. Collective cell migration of epithelial and mesenchymal cells. *Cell. Mol. Life Sci.* 70:3481–92. doi:10.1007/s00018-012-1251-7.

Thievessen, I., P.M. Thompson, S. Berlemont, K.M. Plevock, S. V Plotnikov, A. Zemljic-Harpf, R.S. Ross, M.W. Davidson, G. Danuser, S.L. Campbell, and C.M. Waterman. 2013. Vinculin-actin interaction couples actin retrograde flow to focal adhesions, but is dispensable for focal adhesion growth. *J. Cell Biol.* 202:163–77. doi:10.1083/jcb.201303129.

Tozluoğlu, M., A.L. Tournier, R.P. Jenkins, S. Hooper, P.A. Bates, and E. Sahai. 2013. Matrix geometry determines optimal cancer cell migration strategy and modulates response to interventions. *Nat. Cell Biol.*

Tsygankov, D., C.G. Bilancia, E. a Vitriol, K.M. Hahn, M. Peifer, and T.C. Elston. 2014. CellGeo: A computational platform for the analysis of shape changes in cells with complex geometries. *J. Cell Biol.* 204:443–60. doi:10.1083/jcb.201306067.

Vaughan, L., C.-T. Tan, A. Chapman, D. Nonaka, N.A. Mack, D. Smith, R. Booton, A.F.L. Hurlstone, and A. Malliri. 2014. HUWE1 Ubiquitylates and Degrades the RAC Activator TIAM1 Promoting Cell-Cell Adhesion Disassembly, Migration, and Invasion. *Cell Rep.* 10:88–102. doi:10.1016/j.celrep.2014.12.012.

Vega, F.M., G. Fruhwirth, T. Ng, and A.J. Ridley. 2011. RhoA and RhoC have distinct roles in migration and invasion by acting through different targets. *J. Cell Biol.* 193:655–65. doi:10.1083/jcb.201011038.

White, D.P., P.T. Caswell, and J.C. Norman. 2007. alpha-v beta-3 and alpha-5 beta-1 integrin recycling pathways dictate downstream Rho kinase signaling to regulate persistent cell migration. *J. Cell Biol.* 177:515–25. doi:10.1083/jcb.200609004.

Wu, C., S.B. Asokan, M.E. Berginski, E.M. Haynes, N.E. Sharpless, J.D. Griffith, S.M. Gomez, and J.E. Bear. 2012. Arp2/3 is critical for lamellipodia and response to extracellular matrix cues but is dispensable for chemotaxis. *Cell*. 148:973–987. doi:10.1016/j.cell.2011.12.034.

Zech, T., S.D.J. Calaminus, P. Caswell, H.J. Spence, M. Carnell, R.H. Insall, J. Norman, and L.M. Machesky. 2011. The Arp2/3 activator WASH regulates α5β1-integrin-mediated invasive migration. *J. Cell Sci.* 124:1–7. doi:10.1242/jcs.080986.

Figure Legends

Figure 1: RCP/α5β1 integrin trafficking promotes actin spike formation.

(A) A2780 cells transiently transfected with Lifeact-mRFPmars and paGFP-Actin were seeded onto 3D CDM 4 hrs prior to imaging and treated with cRGDfV (2.5µM, 2hrs) as indicated. ROI1 was photoactivated and cells were imaged every second for 100s. Normalised intensity was analysed for ROI1 (B) and ROI2 (C; n=15 (-cRGDfV), n=16 (+cRGDfV)). Blue bars indicate time points at which datasets are significantly different ($p<0.01$; Student's T-test). Yellow arrows indicate direction of protrusion. (D, E) A2780 cells transiently transfected with Lifeact-mEGFP were seeded as in (A) and Z-stacks captured (7 sections, 0.2µm intervals) on a spinning disk confocal microscope every minute for >25 mins, Z-projections are shown. White arrows indicate lamellipodia-like actin veils, red arrows indicate actin spikes. (F, G) Quantification of Lifeact-mEGFP protrusions. Protrusions were identified by overlapping thresholded movie frames with a lag of 3 minutes. (H) Normalised protrusion size was measured using image masks as represented in (F) and (G). n=28 cells per condition (n>25 frames per cell). (I) A2780 cells were seeded as in (A) before fixation and Alexa488 Phalloidin staining. Structured illumination microscopy (SIM) was used to generate super resolution images, maximum intensity projections are shown. The number (J) and length (K) of filopodia per protrusion was quantified from SIM images, n = 10 cells per condition. All data represent at least 3-independent experiments, statistical significance was evaluated using ANOVA/Tukey's multiple comparison test (H, J, K). + = mean, * = $p < 0.05$, ** = $p < 0.01$.

Figure 2: Dynamic actin spikes form protrusions in cells invading locally *in vivo*.

(A, B) CFSE-labelled A2780 cells or (D, E) H1299 cells were injected into the pericardial cavity of zebrafish embryos, cRGDfV (2.5µM) was added 1 day post-injection (dpi) as appropriate.

Embryos were imaged at 4 dpi to determine invasion. Dashed line indicates the pericardial cavity, A = autofluorescence from the yolk sac, and white arrows indicate invading cells. (C,F) Quantification of relative invasion n=28-33 fish per condition. (G) CFSE labelled A2780 cells stably expressing mRFPmars-Lifeact were injected into zebrafish embryos as in (A,B) and treated with cRGDfV (2.5μM). Imaging was performed 3 dpi using a spinning disk confocal microscope. Images represent Z-projections and 3D rendering. (H) Timelapse of mRFPmars-Lifeact-expressing cells over limited z-range (2.5μm). (I) Kymograph of protrusive area highlighted in (H) (yellow box). White arrowhead indicates an actin spike actively protruding, red arrowhead indicates retraction. Mean grey value indicates intensity of Lifeact fluorescence. White and red arrows highlight dynamic actin spikes. All data represent at least 3-independent experiments, statistical significance was evaluated using Student's T-test with Welch's correction, + = mean, * = $p < 0.05$, *** = $p < 0.001$.

Figure 3: RCP/α5β1-driven migration and invasion is Arp2/3-independent.

(A) siControl, ArpC2 knockdown or ArpC3 knockdown A2780 cells were seeded onto glass coverslips, wounded after 24 hrs and treated with cRGDfV (2.5μM) as indicated prior to fixation. F-actin was stained with FITC-phalloidin and nuclei with DAPI. White arrowheads indicate lamellipodia, red arrowheads indicate non-lamellipodial ruffling protrusions. (B) siControl, ArpC2 knockdown or ArpC3 knockdown A2780 cells were seeded onto 3D CDM for 4 hrs and treated with cRGDfV (2.5μM) where indicated prior to timelapse imaging. (C) Mean square displacement (MSD) measurement of siCtrl, siArpC2 and siArpC3 A2780 cells migrating n CDM. n≥99 cells per condition. (D) Pseudopod length of siCtrl and siArpC2 A2780 cells migrating in CDM. n=100 cells per condition. (E) A2780 cells transiently transfected with mEGFP-Lifeact were seeded onto 3D CDM for 4 hrs, treated with cRGDfV (2.5μM, >2 hrs) and

the indicated inhibitors (50µM) or vehicle control immediately prior to imaging. Maximum Z-projections are shown. White arrowheads indicate lamellipodia, red arrowheads indicate ruffling actin spikes. (F) MSD (n=20) and (G) pseudopod length (n=50) of DMSO, CK-666 and CK-689 treated A2780 cells migrating in CDM. (H) Normalised protrusion size of A2780 cells expressing Lifeact-mEGFP treated with the indicated inhibitor (50µM) as in (E). n=13-21 cells per condition with n≥25 frames quantified per cell. (I) A2780 cells were seeded into an inverted invasion assay in the presence of cRGDfV (2.5µM) where indicated for 72 hrs. DMSO, CK-666 (50µM) and CK-689 (50µM) were added 24 hrs after seeding and imaged 48hrs later to quantify invasion. All data represent at least 3-independent experiments, statistical significance was evaluated using ANOVA/Tukey's multiple comparison test. + = mean, n.s.= not significant, * = $p < 0.05$, ** = $p < 0.01$, **** = $p < 0.0001$.

Figure 4: Formin function is required for protrusion formation.

(A) A2780 cells transiently transfected with Lifeact-mEGFP were seeded onto 3D CDM for 4 hrs, and treated with cRGDfV (2.5µM, 2hrs). Cells were treated with SMIFH2 (25µM) or vehicle control immediately prior to imaging. Maximum Z-projections are shown. White arrowheads indicate lamellipodia-like protrusions, red arrowheads indicate actin spikes and blue arrowheads indicate blebs. (B) Normalised protrusion size of cells as in (A). n=12-20 cells per condition with n≥25 frames quantified per cell. (C) Percentage of movie frames with bleb protrusions, n=17 cells per condition. (D) A2780 cells were seeded into inverted invasion assays in the presence of cRGDfV (2.5µM) where indicated. SMIFH2 (25µM) and vehicle control were added 24 hrs after seeding, and invasion assays imaged for quantification 48hrs later. n=15 per condition. ((E) Formin expression in A2780 cells was measured by qRT-PCR. Gene expression is shown relative to GAPDH expression, n=3. (F) and (G), siRNA miniscreen

of formins in A2780 cells. Migration speed on CDM in the presence of cRGDfV (2.5µM; F) or under basal conditions (G). n=10-30 cells per condition. All data represent at least 3-independent experiments, statistical significance was evaluated using ANOVA/Tukey's multiple comparison test. n.s. = not-significant, + = mean, *= p<0.05, **=p<0.01, ***=p<0.001, **** = p < 0.0001.

Figure 5: FHOD3 drives actin spike formation and migration in 3D matrix.

(A) A2780 cells stably transfected with control or FHOD3 targeting shRNA constructs were lysed, lysates subjected to SDS-PAGE and Western blotting using antibodies specific for FHOD3 and α-tubulin, and analysed using Odyssey. (B) A2780 cells stably expressing shFHOD3 #1, shFHOD3 #2, pLVTHM vector control or RFP-FHOD3 rescue were seeded onto CDM and treated with cRGDfV (2.5µM) where indicated prior to timelapse imaging, and migration speed (B) (n = 96-134 cells per condition) and peudopod length (C) (n=100 cells per condition) were quantified. (D) Representative images of cells from (B) and (C). Asterisks indicate the position of individual cells at different timepoints. (E) A2780 cells stably transfected as in (B) were transiently transfected with Lifeact-mTFP1, seeded onto CDM for 4 hrs and treated with cRGDfV (2.5µM) prior to spinning disk confocal imaging. Maximum Z-projections are shown. Red arrowheads indicate actin spikes, blue arrowheads indicate blebs. (F) Kymographs of yellow boxes in (F). (G) Normalised protrusion size of cells (n=23-28 cells per condition) and (H) percentage of movie frames with bleb protrusions (n=30 cells per condition). All data represent at least 3-independent experiments, statistical significance was evaluated using ANOVA/Tukey's multiple comparison test. *=p<0.05, **=p<0.01, ***=p<0.001, ****=p<0.0001.

Figure 6: ROCK phosphorylates FHOD3 and promotes formation of actin spike protrusions.

(A) A2780 cells stably expressing RFP or RFP-FHOD3/shFHOD3#1 were untreated or treated with cRDGfV (2.5μM, 30mins) and ROCK inhibitor Gly-H1152 (100nM, 30 mins) or Rho inhibitor I (4μg/ml, 4 hours) as indicated. RFP trap was performed from cell lysates, and subjected to SDS-PAGE and Western blotting using RFP and pS/T antibodies. Fluorescence intensity of pS/T bands was measured using ImageJ, and expressed relative to untreated (n>4 per condition). (B) A2780 cells were seeded onto CDMs and treated with cRGDfV (2.5μM) and ROCK inhibitor Gly-H1152 (100nM) where indicated prior to timelapse imaging. Asterisks indicate the position of individual cells at different timepoints. (C) Migration speed was measured for cells treated as in (B); n=150 cells per condition. (D, E) A2780 cells transiently transfected with Lifeact-mEGFP were seeded onto 3D CDM for 4 hrs and cRGDfV (2.5μM, 2hrs) and Gly-H1152 added as indicated. Z-stacks were captured on a spinning disk confocal microscope every minute for ≥25 mins. Z-projections are shown. White arrows indicate lamellipodia-like actin veils, red arrows indicate actin spikes. (E) Normalised protrusion size was measured for cells in (D), n=21-27 cells per condition. All data represent at least 3-independent experiments, statistical significance was evaluated using ANOVA/Tukey's multiple comparison test. + = mean, n.s. = not significant, * = $p < 0.05$, ** = $p < 0.01$, *** = $p < 0.001$, **** = $p < 0.0001$.

Figure 7: FHOD3 phosphorylation is required for actin spike protrusions and migration in 3D CDM.

(A) A2780 cells stably expressing RFP or RFP-FHOD3 wt/3A/3D were treated with cRDGfV (2.5mM, 30mins), and RFP trap as in 6A. Fluorescence intensity of pS/T bands was measured using ImageJ, and expressed relative to untreated (n=4 per condition). (B) A2780 cells were

seeded onto CDM and treated with cRGDfV (2.5µM) and ROCK inhibitor Gly-H1152 (100nM) where indicated prior to timelapse imaging. Asterisks indicate the position of individual cells at different timepoints. (C) Migration speed was determined for cells treated as in (B); n>60 cells per condition. (D) A2780 cells stably expressing RFP/pLVTHM, RFP-FHOD3 3A/shFHOD3#1 or RFP-FHOD3 3D/shFHOD3#1 were transiently transfected with Lifeact-mTFP1, seeded onto CDM for 4 hrs and treated with cRGDfV (2.5µM) prior to spinning disk confocal imaging. Maximum Z-projections are shown. (E) Kymograph analysis of (D), highlighted with yellow boxes. (F) Normalised protrusion size of cells in (D), n=22-27 cells per condition. All data represent at least 3-independent experiments, statistical significance was evaluated using ANOVA/Tukey's multiple comparison test. + = mean, **=p<0.01, ***=p<0.001.

Figure 8: FHOD3 is required for invasive migration *in vitro* and *in vivo*.

(A) A2780 cells stably expressing pLVTHM vector control, shFHOD3 #1 or shFHOD3 #2 were seeded into inverted invasion assays and allowed to invade into Collagen-I/fibronectin matrix for 72 hours. Cells were visualised with calcein-AM and and serial confocal sections captured at 15µm intervals. (B) Invasion of H1299-p53-273H cells stably expressing pLVTHM vector control, shFHOD3 #1 or shFHOD3 #2 was determined as in (A). (C) A2780 cells stably expressing pLVTHM vector control, shFHOD3 #1 or shFHOD3 #2 were injected into the pericardial cavity of zebrafish embryos and treated with cRGDfV (2.5µM). White arrows indicate invading cells. Dashed line indicates pericardial cavity. (D) Relative invasion quantification of (C), n = 24-27 fish per condition. All data represent at least 3-independent experiments, statistical significance was evaluated using ANOVA/Tukey's multiple comparison test. + = mean, * = p<0.05, ** = p <0.01, **** = p<0.0001.

Figure S1: Mutant p53-expressing cells display limited retrograde actin flow at the leading edge.

(A) A2780 cells transiently transfected with Lifeact-mRFPmars and paGFP-Actin or paGFP were seeded onto glass-bottomed dishes 24 hrs prior to imaging and treated with cRGDfV (2.5µM, 2hrs) as indicated. ROI1 was photoactivated and cells were imaged every second for 100s. Normalised intensity was analysed for ROI1 and ROI2 (n=21 (-cRGDfV), n=20 (+cRGDfV)). (B) H1299-Vec and H1299-p53-273H cells transfected as in (A) were seeded onto glass-bottomed dishes 24 hrs prior to imaging. Photoactivation was performed as in (A; n=15 (VEC), n=10 (p53-273H)). (C) MDA-MB-231 cells transfected as in (A) were seeded onto CDM-coated glass-bottomed dishes 4 hrs prior to imaging. Photoactivation was performed as in (A; n=10). Yellow arrows indicate direction of protrusion, error bars represent SEM. All data represent at least 3-independent experiments. Blue bars indicate time points at which -/+cRGDfV or mutant p53 datasets are significantly different ($p<0.01$; Student's T-test).

Figure S2: Mutant p53-expressing cells generate bursts of actin spikes.

(A) H1299-Vec, (B) H1299-p53-273H or (C) MDA-MB-231 cells transiently transfected with mEGFP-Lifeact were seeded onto CDMs for 4 hrs and imaged using a spinning disk confocal microscope every minute for >25 mins. Z-projections are shown. White arrows indicate lamellipodial protrusions, red arrows indicate actin spikes. (D) A2780 cells transfected with mEGFP-Lifeact were seeded onto CDMs for 4 hrs and imaged using a spinning disk confocal microscope every minute for 15 minutes and filopodia lifetime was analysed, n=8 cells per condition. All data represent at least 3-independent experiments, statistical significance was evaluated using Student's T-test with Welch's correction. + =mean, * = $p < 0.05$.

Figure S3: Arp2/3 is not required for RCP/α5β1-driven migration in 2D and 3D.

(A) A2780 cells were seeded onto tissue culture plates 24 hrs prior to wounding. Cells were treated with cRGDfV (2.5μM), DMSO, CK-666 or CK-689 (50μM) as indicated prior to timelapse imaging. White arrows indicate lamellipodia, red arrows indicate non-lamellipodial ruffling protrusions. Migration speed (B), directional persistence (C) and autocorrelation (D) of cells migrating in 2D treated as in (A). n=20 cells per condition. (E) A2780 cells were prepared as in (A) and treated with cRGDfV (2.5μM), DMSO or CK-666 (50μM or 100μM) as indicated prior to timelapse imaging. 2D migration speed was analysed, n=35 cells per condition. (F) Mouse embryonic fibroblasts (MEF) were seeded onto tissue culture plates 24 hrs prior to wounding. Cells were treated withDMSO, CK-689 (100 μM) or CK-666 (50μM or 100μM) as indicated prior to timelapse imaging. 2D migration speed was analysed, n=75 cells per condition. (G) A2780 cells were seeded onto CDM for 4 hrs and treated with cRGDfV (2.5μM) and DMSO, CK-666 or CK-689 (50μM) as indicated prior to timelapse imaging. 3D migration speed was analysed. n=20 cells per condition. (H) siRNA SMARTpool knockdown of ArpC2 and ArpC3 in A2780 cells. (I) 3D migration speed of siCtrl, siArpC2 and siArpC3 A2780 cells migrating in CDM (as in Figure 3C). n≥99 cells per condition. (J) Distance from the rear of the cell to the centre of the nucleus of siCtrl and siArpC2 A2780 cells migrating in CDM. n=100 cells per condition. (K) α5 integrin recycling in A2780 cells was measured upon treatment with CK-666 or CK-689 (50μM), n=24 wells over 3 experiments. (L) GFP-RCP transfected A2780 cells were seeded onto CDMs for 4 hours prior to treatment with cRGDfV (2.5μM), CK-666 or CK-689 (50μM) as indicated prior to confocal imaging. Bounding boxes around the cell perimeter (yellow) were used to identify the front and rear quarter (green or red, respectively) of the cell, and % GFP-RCP intensity at the front measured (M), n=15-28 cells per condition. All data

represent at least 3-independent experiments, statistical significance was evaluated using ANOVA/Tukey's multiple comparison test. + = mean. n.s. = not significant, *=p<0.05, **=p<0.01, ***=p<0.001, ****=p<0.0001.

Figure S4: FHOD3 is required for 3D (but not 2D) migration.

(A) Percentage knockdown of formins expressed in A2780 cells by siRNA, measured by qRT-PCR. n=2-3 per condition. (B) A2780 cells were stably transfected with pLVTHM vector control, shFHOD3 #1 or shFHOD3 #2. shFHOD3 #1 was rescued with sh-resistant RFP-FHOD3. FHOD3 gene expression was measured by qRT-PCR. Fold change in gene expression relative to pLVTHM vector control. n=3-6 independent experiments. (C) A2780 cells stably expressing pLVTHM vector control, shFHOD3 #1 or shFHOD3 #2 were seeded onto tissue culture plates 24 hrs prior to wounding. Cells were treated with cRGDfV (2.5μM) as indicated prior to timelapse imaging. Quantification of 2D migration speed, (D) directional persistence and (E) autocorrelation, n=45-70 cells per condition. (F) A2780 cells stably expressing shFHOD3 #1, shFHOD3 #2, pLVTHM vector control or RFP-FHOD3 rescue were seeded onto CDM and treated with cRGDfV (2.5μM) where indicated prior to timelapse imaging, and mean square displacement (MSD) was quantified; n=96-134 cells per condition. (G) RNA extracted from cell lines as indicated was used as to determine FHOD3 isoforms expressed by RT-PCR, using primers specific for non-muscle and muscle specific isoforms of FHOD3 (pan FHOD3, to yield products at 478bp and 502bp respectively) or muscle specific FHOD3 primers (to yield a product at 316bp). All data represent at least 3-independent experiments, statistical significance was evaluated using ANOVA/Tukey's multiple comparison test. + = mean, n.s. = not significant, **=p<0.01, ****=p<0.0001.

Figure S5: Wild-type FHOD3 localises to actin filaments in 3D CDM; active FHOD3 localises to actin spikes in 3D CDM.

(A) A2780 cells stably expressing RFP or RFP-FHOD3 were seeded onto CDMs for 4 hours and treated with cRGDfV (2.5µM) where indicated. Cells were fixed and stained with anti-RFP antibody and Alexa Fluor 647-conjugated-phalloidin prior to widefield fluorescence imaging. Arrows indicate localisation of RFP-FHOD3 on actin filaments. (B) A2780 cells were transiently transfected with GFP or GFP-FHOD3ΔDAD, seeded onto CDMs for 4 hours and treated with cRGDfV (2.5µM) where indicated. Cells were fixed and stained with TRITC-phalloidin prior to spinning disk confocal imaging. Arrows indicate colocalisation of actin spikes and GFP-FHOD3ΔDAD. Dashed lines indicate line profile intensity measurements in (C). (D) H1299-273H cells were stably transfected with pLVTHM vector control, shFHOD3 #1 or shFHOD3 #2. Cells were lysed; lysates were subjected to SDS-PAGE and Western blotting using antibodies specific for FHOD3 and α-tubulin. All data represent at least 3-independent experiments.

Movie Legends

Movie 1: Retrograde actin flow is slowed within actin-based protrusions formed during RCP/α5β1-driven migration.

A2780 cells transiently transfected with Lifeact-mRFPmars and paGFP-Actin were seeded onto 3D CDM 4 hrs prior to imaging and treated with cRGDfV (2.5µM, 2hrs) as indicated. ROI1 (Figure 1D) was photoactivated and cells were imaged every second for 100s. Frame rate 7fps.

Movie 2: RCP/α5β1 integrin trafficking promotes actin spike formation.

A2780 cells transiently transfected with Lifeact-mEGFP were seeded onto 3D CDM for 4 hrs and cRGDfV (2.5µM, 2hrs) added as appropriate. Z-stacks were captured (7 sections, 0.2µm

intervals) on a spinning disk confocal microscope every minute for 45 mins. Z-projection movies are shown, frame rate 7fps.

Movie 3: Dynamic actin spikes form protrusions in cells invading locally *in vivo*.

A2780 cells stably expressing Lifeact-mRFPMars were injected into the pericardial cavity of zebrafish embryos and cRGDfV (2.5μM) was added 1 day post-injection (dpi). Imaging was performed at 3dpi using a spinning disk confocal microscope; Z-stacks were captured (7 sections, 0.5 μm intervals) on a spinning disk confocal microscope every 15s for 15 mins. Z-projection movies are shown, frame rate 7fps.

Movie 4: Arp2/3 activity is not required for RCP/α5β1 driven actin spike formation.

A2780 cells transiently transfected with Lifeact-mEGFP were seeded onto 3D CDM for 4 hrs, and treated with cRGDfV (2.5μM >2 hrs). Cells were treated with the indicated inhibitors (50μM) or vehicle control immediately prior to imaging. Z-stacks were captured (7 sections, 0.2μm intervals) on a spinning disk confocal microscope every minute for 15 mins. Z-projection movies are shown, frame rate 7fps.

Movie 5: FHOD3 is required for RCP/α5β1 driven actin spike formation.

A2780 cells stably expressing shFHOD3 #1, shFHOD3 #2, pLVTHM vector control or RFP-FHOD3 rescue were transiently transfected with Lifeact-mTFP1 and seeded onto CDM for 4 hrs and treated with cRGDfV (2.5μM). Z-stacks were captured (7 sections, 0.2μm intervals) on a spinning disk confocal microscope every minute for 15 mins. Z-projection movies are shown, frame rate 7fps.

Movie 6: ROCK is required for RCP/α5β1 driven actin spike formation.

A2780 cells stably expressing were transiently transfected with Lifeact-mTFP1 and seeded onto CDM for 4 hrs and treated with cRGDfV (2.5µM) in the presence or absence of the ROCK inhibitor Gly-H-1152. Z-stacks were captured (7 sections, 0.2µm intervals) on a spinning disk confocal microscope every minute for 15 mins. Z-projection movies are shown, frame rate 7fps.

Movie 7: RFP-FHOD3-3A does not support actin spike formation.

A2780 cells stably expressing shFHOD3 #1 along with RFP or RFP-FHOD3 3A/3D rescue were transiently transfected with Lifeact-mTFP1 and seeded onto CDM for 4 hrs and treated with cRGDfV (2.5µM) i. Z-stacks were captured (7 sections, 0.2µm intervals) on a spinning disk confocal microscope every minute for 15 mins. Z-projection movies are shown, frame rate 7fps.

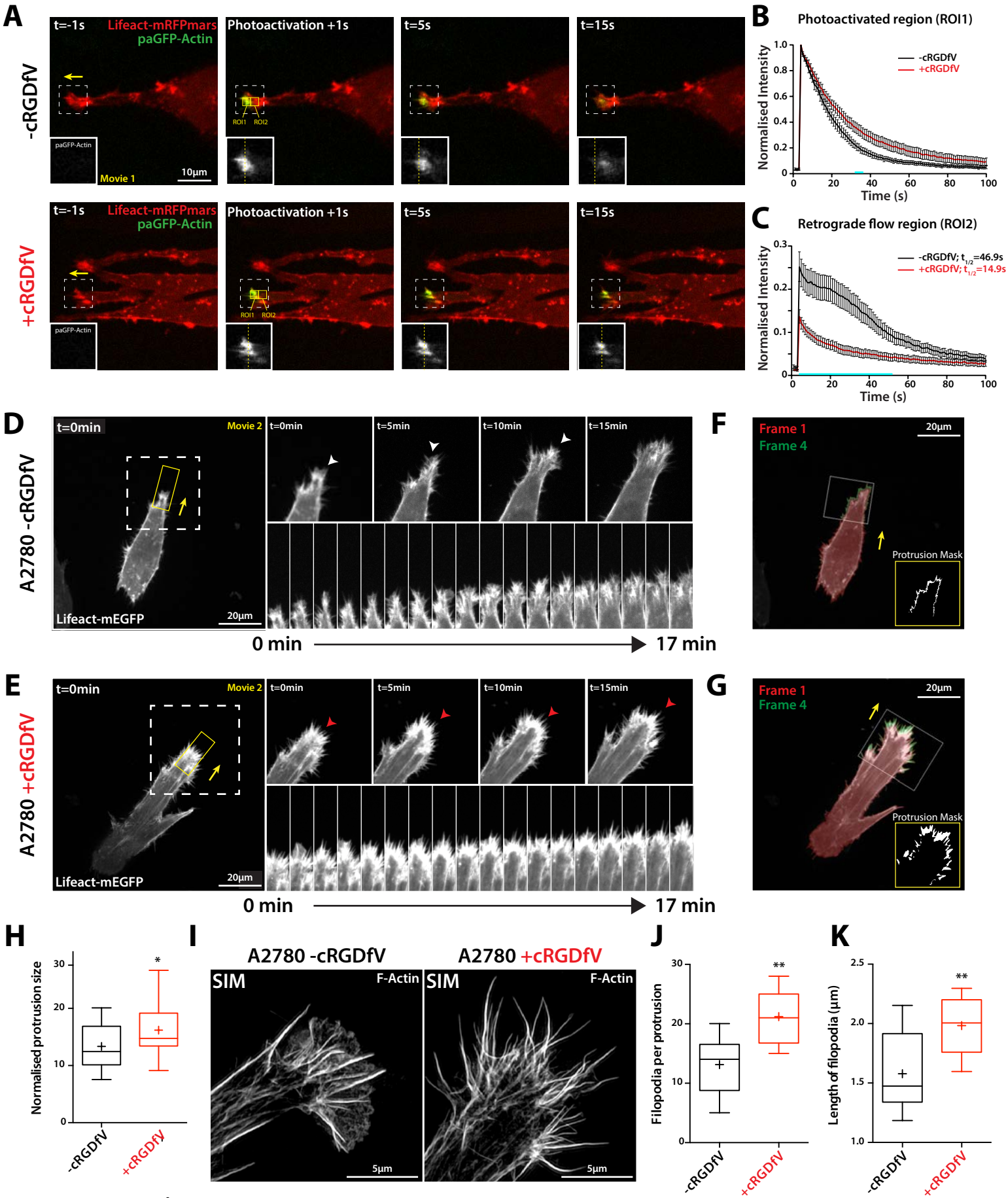

Figure 1: RCP/α5β1 integrin trafficking promotes actin spike formation.

(A) A2780 cells transiently transfected with Lifeact-mRFPmars and paGFP-Actin were seeded onto 3D CDM 4 hrs prior to imaging and treated with cRGDfV (2.5µM, 2hrs) as indicated. ROI1 was photoactivated and cells were imaged every second for 100s. Normalised intensity was analysed for ROI1 (B) and ROI2 (C; n=15 (-cRGDfV), n=16 (+cRGDfV)). Blue bars indicate time points at which datasets are significantly different ($p<0.01$; Student's T-test). Yellow arrows indicate direction of protrusion. (D, E) A2780 cells transiently transfected with Lifeact-mEGFP were seeded onto 3D CDM for 4 hrs and cRGDfV (2.5µM, 2hrs) added as appropriate. Z-stacks were captured (7 sections, 0.2µm intervals) on a spinning disk confocal microscope every minute for >25 mins, Z-projections are shown. White arrows indicate lamellipodia-like actin veils, red arrows indicate actin spikes. (F, G) Quantification of Lifeact-mEGFP protrusions. Protrusions were identified by overlapping thresholded movie frames with a lag of 3 minutes. (H) Normalised protrusion size was measured using image masks as represented in (F) and (G). n=28 cells per condition (n>25 frames per cell). (I) A2780 cells were seeded onto CDM and treated with cRGDfV (2.5µM, 2hrs) before fixation and Alexa488 Phalloidin staining. Structured illumination microscopy (SIM) was used to generate super resolution images, maximum intensity projections are shown. The number (J) and length (K) of filopodia per protrusion was quantified from SIM images, n = 10 cells per condition. All data represent at least 3-independent experiments, statistical significance was evaluated using ANOVA/Tukey's multiple comparison test (H, J, K). + = mean, * = $p < 0.05$, ** = $p < 0.01$.

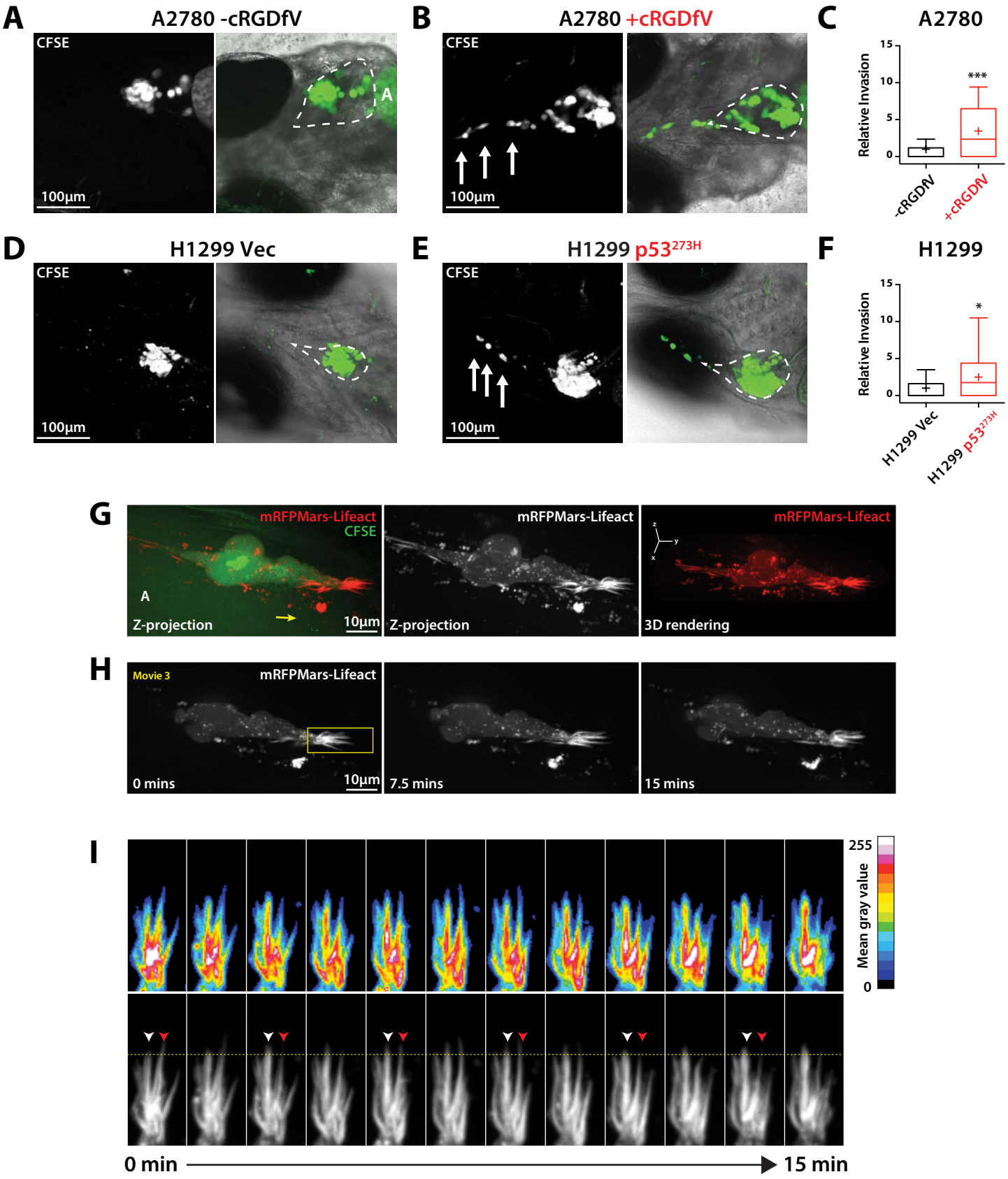

Figure 2: Dynamic actin spikes form protrusion in cells invading locally *in vivo.*

(A, B) CFSE-labelled A2780 cells or (D, E) H1299 cells were injected into the pericardial cavity of zebrafish embryos, cRGDfV (2.5µM) was added 1 day post-injection (dpi) as appropriate. Embryos were imaged at 4 dpi to determine invasion. Dashed line indicates the pericardial cavity, A = autofluorescence from the yolk sac, and white arrows indicate invading cells. (C,F) Quantification of relative invasion n=28-33 fish per condition. (G) CFSE labelled A2780 cells stably expressing mRFPmars-Lifeact were injected into zebrafish embryos as in (A,B) and treated with cRGDfV (2.5µM). Imaging was performed 3 dpi using a spinning disk confocal microscope. Images represent Z-projections and 3D rendering of a z-stack though the entire volume of the cell. (H) Timelapse of mRFPmars-Lifeact-expressing cells over limited z-range (2.5µm). (I) Kymograph of protrusive area highlighted in (H) (yellow box). White arrowhead indicates an actin spike actively protruding, red arrowhead indicates retraction. Mean grey value indicates intensity of Lifeact fluorescence. White and red arrows highlight dynamic actin spikes. All data represent at least 3-independent experiments, statistical significance was evaluated using Student's T-test with Welch's correction, + = mean, * = $p < 0.05$, *** = $p < 0.001$.

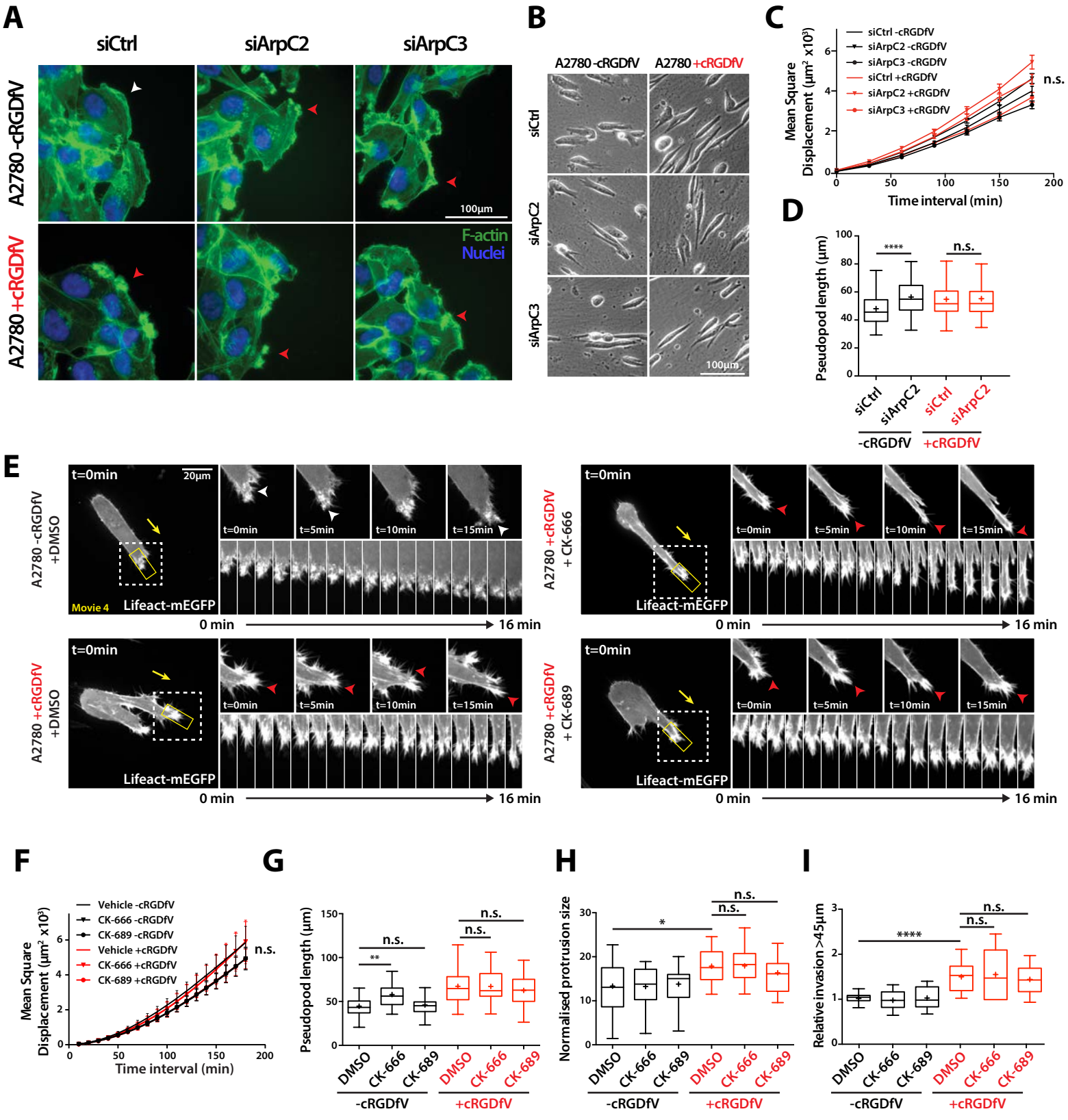

Figure 3: RCP/α5β1-driven migration and invasion is Arp2/3-independent.

(A) siControl, ArpC2 knockdown or ArpC3 knockdown A2780 cells were seeded onto glass coverslips, wounded after 24 hrs and treated with cRGDfV (2.5µM) as indicated prior to fixation. F-actin was stained with FITC-phalloidin and nuclei with DAPI. White arrowheads indicate lamellipodia, red arrowheads indicate non-lamellipodial ruffling protrusions. (B) siControl, ArpC2 knockdown or ArpC3 knockdown A2780 cells were seeded onto 3D CDM for 4 hrs and treated with cRGDfV (2.5µM) where indicated prior to timelapse imaging. (C) Mean square displacement (MSD) measurement of siCtrl, siArpC2 and siArpC3 A2780 cells migrating n CDM. n≥99 cells per condition. (D) Pseudopod length of siCtrl and siArpC2 A2780 cells migrating in CDM. n=100 cells per condition. (E) A2780 cells transiently transfected with mEGFP-Lifeact were seeded onto 3D CDM for 4 hrs, treated with cRGDfV (2.5µM, >2 hrs) and the indicated inhibitors (50µM) or vehicle control immediately prior to imaging. Maximum Z-projections are shown. White arrowheads indicate lamellipodia, red arrowheads indicate ruffling actin spikes. (F) MSD (n=20) and (G) pseudopod length (n=50) of DMSO, CK-666 and CK-689 treated A2780 cells migrating in CDM. (H) Normalised protrusion size of A2780 cells expressing Lifeact-mEGFP treated with the indicated inhibitor (50µM) as in (E). n=13-21 cells per condition with n≥25 frames quantified per cell. (I) A2780 cells were seeded into an inverted invasion assay in the presence of cRGDfV (2.5µM) where indicated for 72 hrs. DMSO, CK-666 (50µM) and CK-689 (50µM) were added 24 hrs after seeding and imaged 48hrs later to quantify invasion. All data represent at least 3-independent experiments, statistical significance was evaluated using ANOVA/Tukey's multiple comparison test. + = mean, n.s.= not significant, * = $p < 0.05$, ** = $p < 0.01$, **** = $p < 0.0001$.

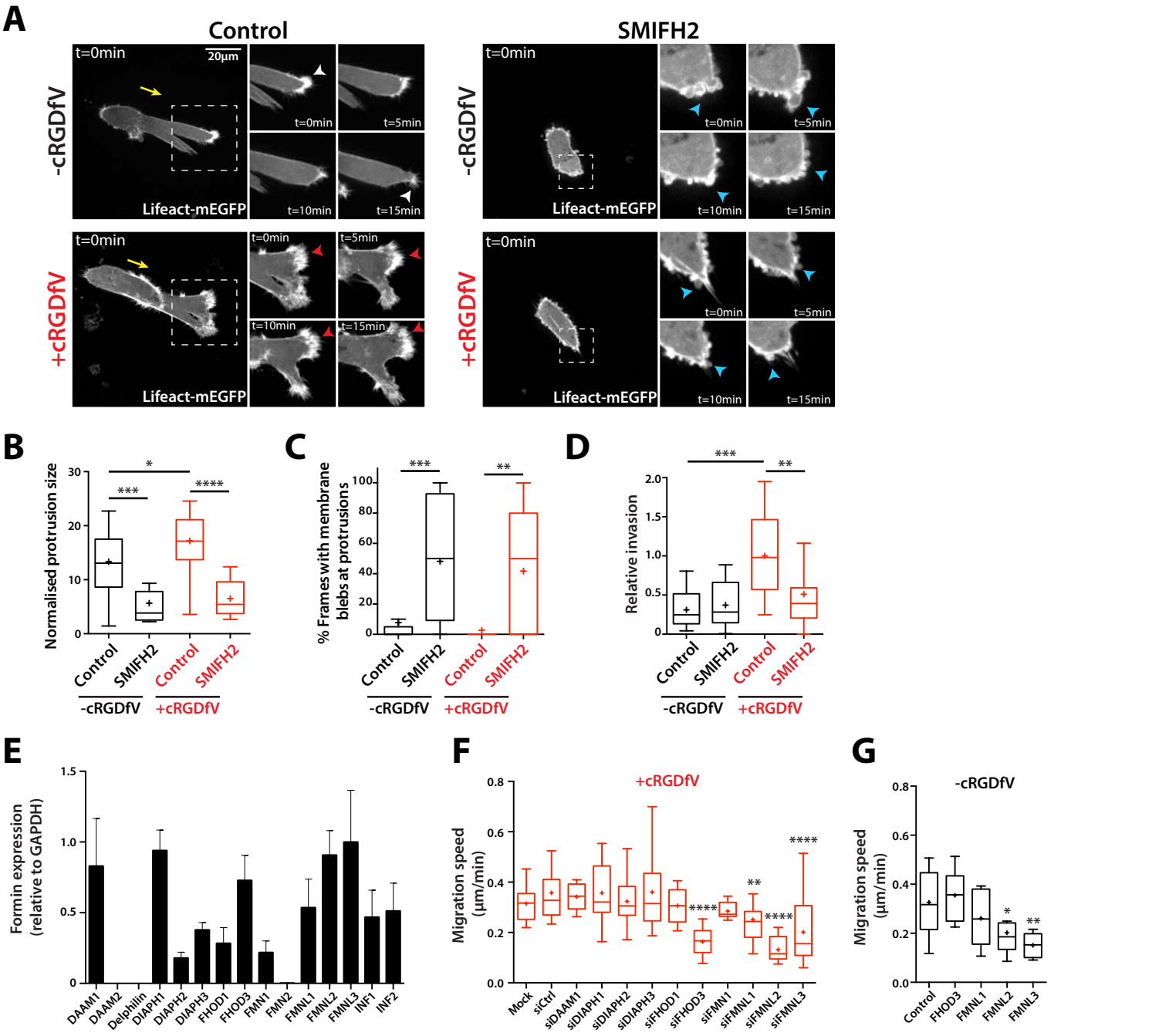

Figure 4: Formin function is required for protrusion formation.

(A) A2780 cells transiently transfected with Lifeact-mEGFP were seeded onto 3D CDM for 4 hrs, and treated with cRGDfV (2.5μM, 2hrs). Cells were treated with SMIFH2 (25μM) or vehicle control immediately prior to imaging. Maximum Z-projections are shown. White arrowheads indicate lamellipodia-like protrusions, red arrowheads indicate actin spikes and blue arrowheads indicate blebs. (B) Normalised protrusion size of cells as in (A). n=12-20 cells per condition with n≥25 frames quantified per cell. (C) Percentage of movie frames with bleb protrusions, n=17 cells per condition. (D) A2780 cells were seeded into inverted invasion assays in the presence of cRGDfV (2.5μM) where indicated. SMIFH2 (25μM) and vehicle control were added 24 hrs after seeding, and invasion assays imaged for quantification 48hrs later. n=15 per condition. ((E) Formin expression in A2780 cells was measured by qRT-PCR. Gene expression is shown relative to GAPDH expression, n=3. (F) and (G), siRNA miniscreen of formins in A2780 cells. Migration speed on CDM in the presence of cRGDfV (2.5μM; F) or under basal conditions (G). n=10-30 cells per condition. All data represent at least 3-independent experiments, statistical significance was evaluated using ANOVA/Tukey's multiple comparison test. n.s. = not-significant, + = mean, *= p<0.05, **=p<0.01, ***=p<0.001, **** = p < 0.0001.

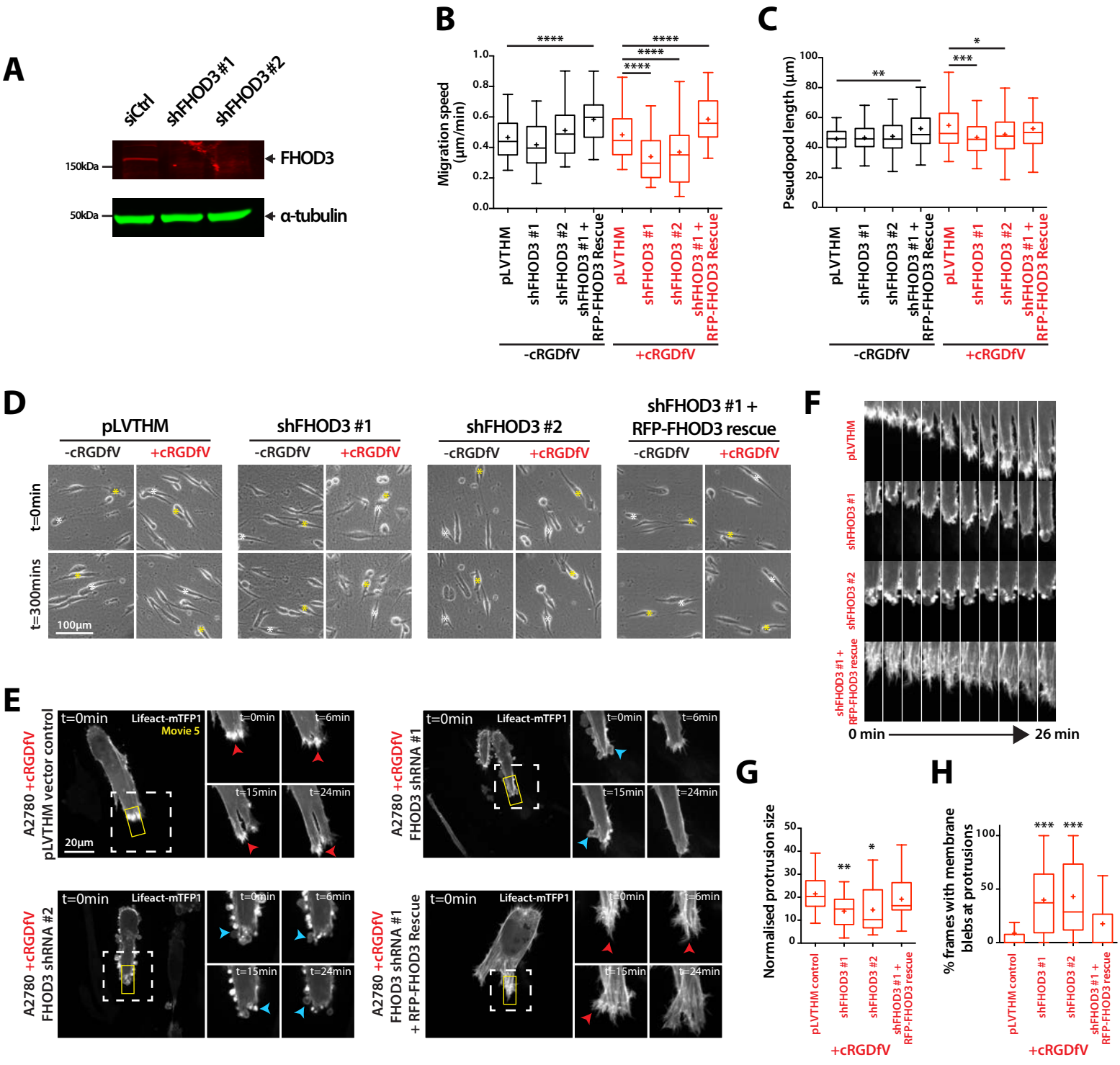

Figure 5: FHOD3 drives actin spike formation and migration in 3D matrix.

(A) A2780 cells were stably transfected with control or FHOD3 targeting shRNA constructs. Cells were lysed, lysates subjected to SDS-PAGE and Western blotting using antibodies specific for FHOD3 and a-tubulin, and analysed using Odyssey. (B) A2780 cells stably expressing shFHOD3 #1, shFHOD3 #2, pLVTHM vector control or RFP-FHOD3 rescue were seeded onto CDM and treated with cRGDfV (2.5μM) where indicated prior to timelapse imaging, and migration speed (B) (n = 96-134 cells per condition) and peudopod length (C) (n=100 cells per condition) were quantified. (D) Representative images of cells from (B) and (C). Asterisks indicate the position of individual cells at different timepoints. (E) A2780 cells stably expressing shFHOD3 #1, shFHOD3 #2, pLVTHM vector control or RFP-FHOD3 rescue were transiently transfected with Lifeact-mTFP1, seeded onto CDM for 4 hrs and treated with cRGDfV (2.5μM) prior to spinning disk confocal imaging. Maximum Z-projections are shown. Red arrowheads indicate actin spikes, blue arrowheads indicate blebs. (F) Kymographs of yellow boxes in (F). (G) Normalised protrusion size of cells (n=23-28 cells per condition) and (H) percentage of movie frames with bleb protrusions (n=30 cells per condition). All data represent at least 3-independent experiments, statistical significance was evaluated using ANOVA/Tukey's multiple comparison test. *=p<0.05, **=p<0.01, ***=p<0.001, ****=p<0.0001.

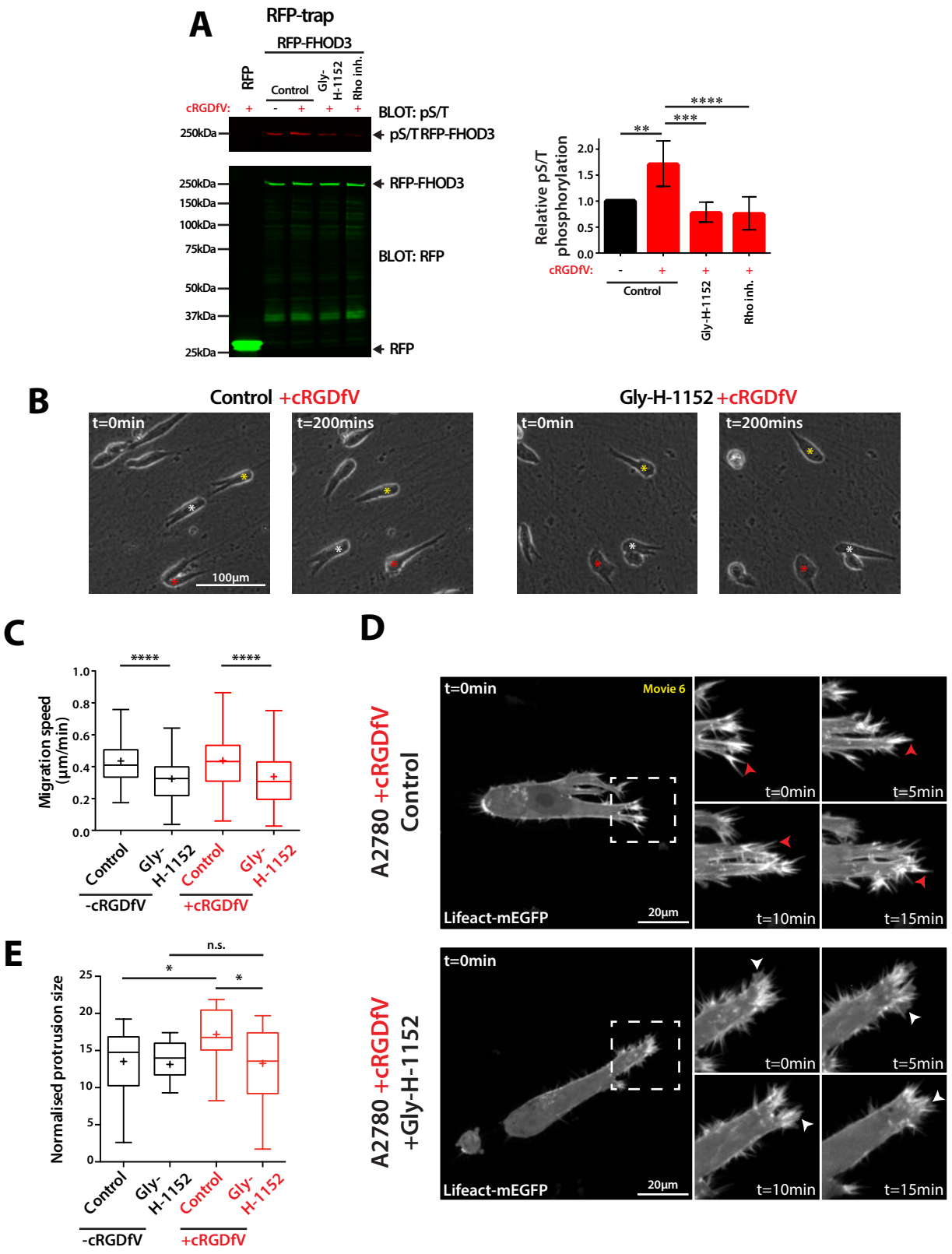

Figure 6: ROCK phosphorylates FHOD3 and promotes formation of actin spike protrusions

(A) A2780 cells stably expressing RFP or RFP-FHOD3/shFHOD3#1 were untreated or treated with cRDGfV (2.5µM, 30mins) and ROCK inhibitor Gly-H1152 (100nM, 30 mins) or Rho inhibitor I (4µg/ml, 4 hours) as indicated. RFP trap was performed from cell lysates, and subjected to SDS-PAGE and Western blotting using RFP and pS/T antibodies. Fluorescence intensity of pS/T bands was measured using ImageJ, and expressed relative to untreated (n>4 per condition). (B) A2780 cells were seeded onto CDMs and treated with cRGDfV (2.5µM) and ROCK inhibitor Gly-H1152 (100nM) where indicated prior to timelapse imaging. Asterisks indicate the position of individual cells at different timepoints. (C) Migration speed was measured for cells treated as in (B); n=150 cells per condition. (D, E) A2780 cells transiently transfected with Lifeact-mEGFP were seeded onto 3D CDM for 4 hrs and cRGDfV (2.5µM, 2hrs) and Gly-H1152 added as indicated. Z-stacks were captured on a spinning disk confocal microscope every minute for ≥25 mins. Z-projections are shown. White arrows indicate lamellipodia-like actin veils, red arrows indicate actin spikes. (E) Normalised protrusion size was measured for cells in (D), n=21-27 cells per condition. All data represent at least 3-independent experiments, statistical significance was evaluated using ANOVA/Tukey's multiple comparison test. + = mean, n.s. = not significant, * = $p < 0.05$, ** = $p < 0.01$, *** = $p < 0.001$, **** = $p < 0.0001$.

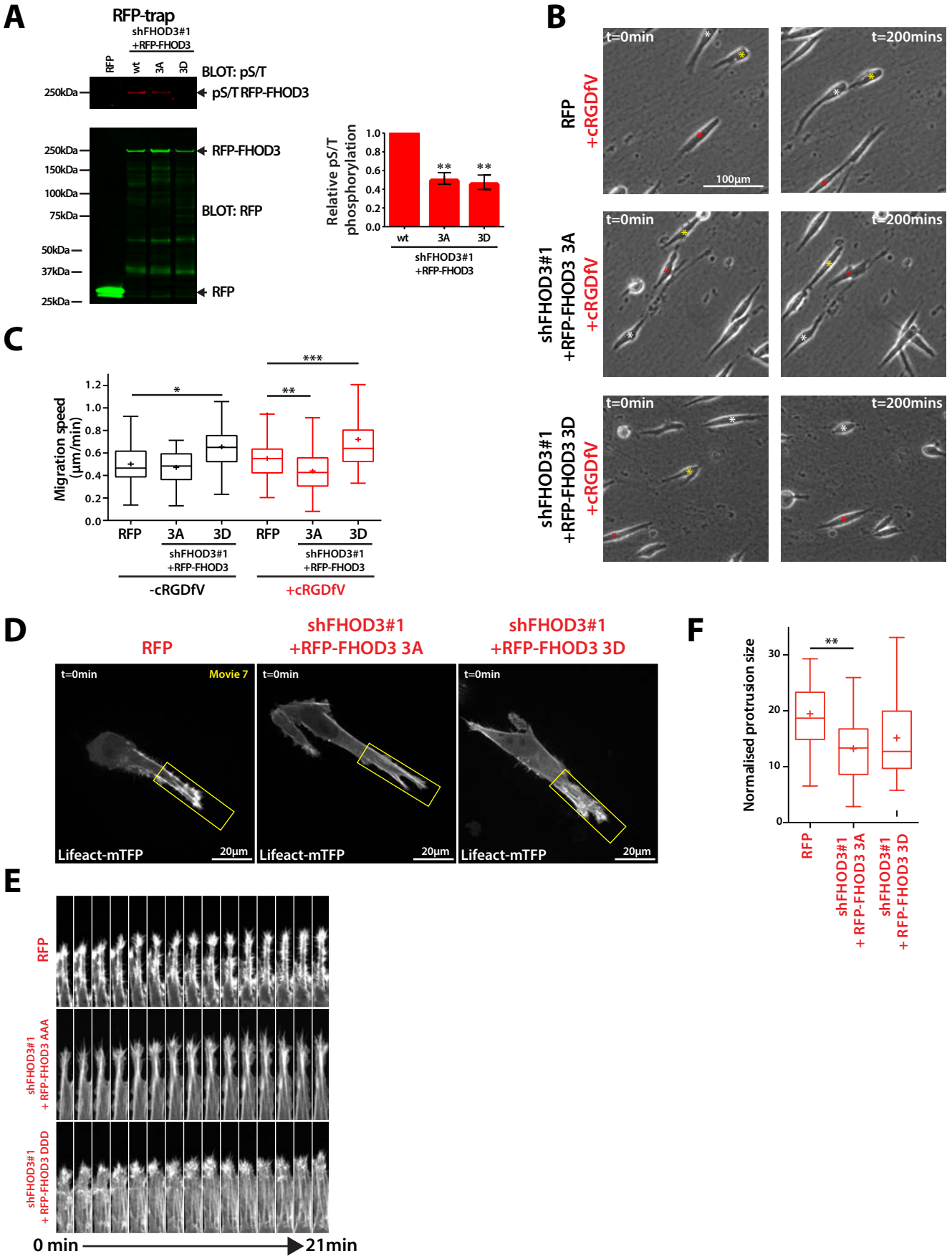

Figure 7: FHOD3 phosphorylation is required for actin spike protrusions and migration in 3D CDM

(A) A2780 cells stably expressing RFP or RFP-FHOD3 wt/3A/3D were treated with cRDGfV (2.5mM, 30mins), and RFP trap was performed from cell lysates and subjected to SDS-PAGE and Western blotting using RFP and pS/T antibodies. Fluorescence intensity of pS/T bands was measured using ImageJ, and expressed relative to untreated (n=4 per condition). (B) A2780 cells were seeded onto CDM and treated with cRGDfV (2.5µM) and ROCK inhibitor Gly-H1152 (100nM) where indicated prior to timelapse imaging. Asterisks indicate the position of individual cells at different timepoints. (C) Migration speed was determined for cells treated as in (B); n>60 cells per condition. (D) A2780 cells stably expressing RFP/pLVTHM, RFP-FHOD3 3A/shFHOD3#1 or RFP-FHOD3 3D/shFHOD3#1 were transiently transfected with Lifeact-mTFP1, seeded onto CDM for 4 hrs and treated with cRGDfV (2.5µM) prior to spinning disk confocal imaging. Maximum Z-projections are shown. (E) Kymograph analysis of (D), highlighted with yellow boxes. (F) Normalised protrusion size of cells in (D), n=22-27 cells per condition. All data represent at least 3-independent experiments, statistical significance was evaluated using ANOVA/Tukey's multiple comparison test. + = mean, **=p<0.01, ***=p<0.001.

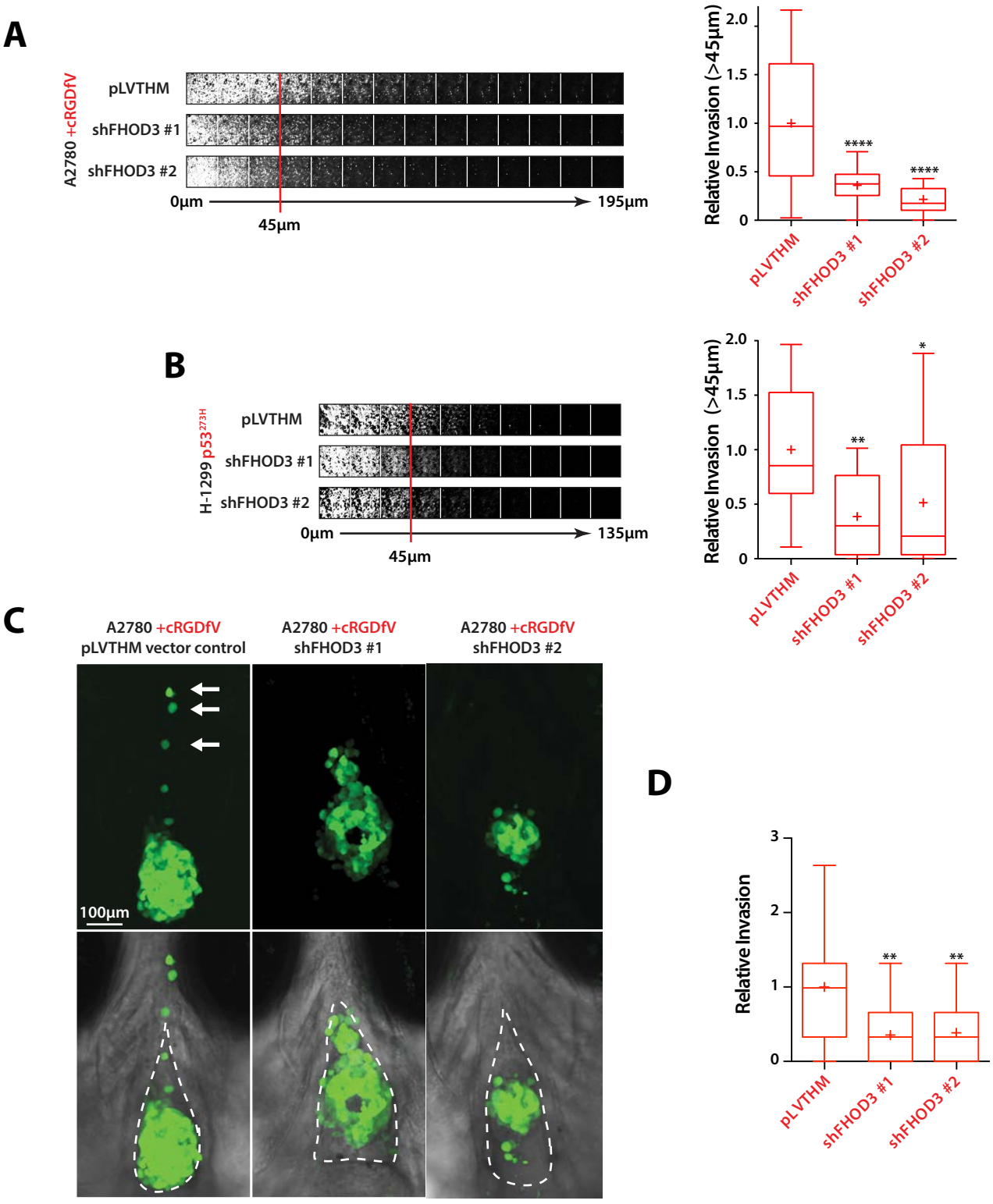

Figure 8: FHOD3 is required for invasive migration *in vitro* and *in vivo*.

(A) A2780 cells stably expressing pLVTHM vector control, shFHOD3 #1 or shFHOD3 #2 were seeded into inverted invasion assays and allowed to invade into Collagen-I/fibronectin matrix for 72 hours. Cells were visualised with calcein-AM and and serial confocal sections captured at 15µm intervals. (B) Invasion of H1299-p53-273H cells stably expressing pLVTHM vector control, shFHOD3 #1 or shFHOD3 #2 was determined as in (A). (C) A2780 cells stably expressing pLVTHM vector control, shFHOD3 #1 or shFHOD3 #2 were injected into the pericardial cavity of zebrafish embryos and treated with cRGDfV (2.5µM). White arrows indicate invading cells. Dashed line indicates pericardial cavity. (D) Relative invasion quantification of (C), n = 24-27 fish per condition. All data represent at least 3-independent experiments, statistical significance was evaluated using ANOVA/Tukey's multiple comparison test. + = mean, * = p<0.05, ** = p <0.01, **** = p<0.0001.

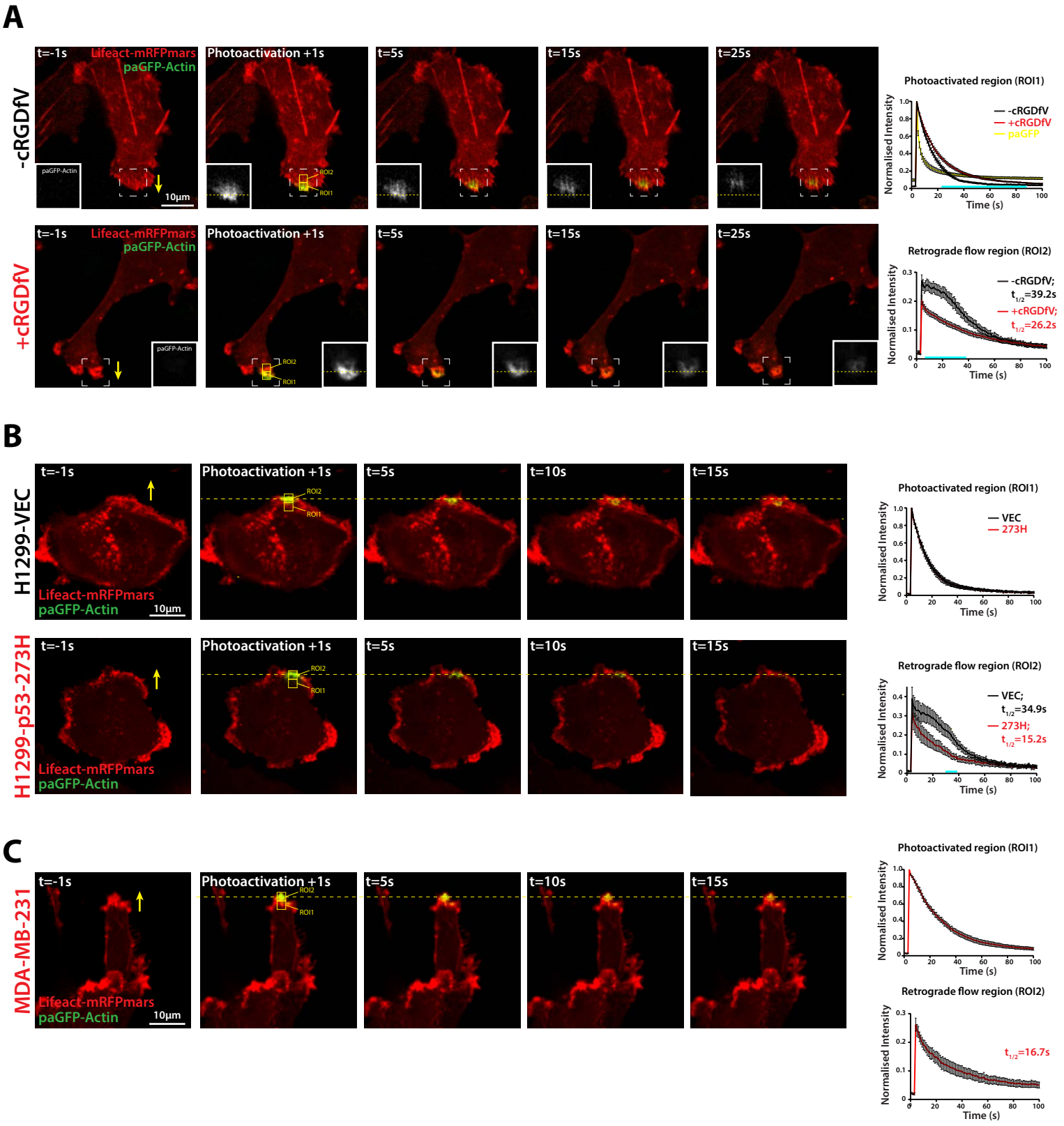

Figure S1: Mutant p53 expressing cells display limited retrograde actin flow at the leading edge.

(A) A2780 cells transiently transfected with Lifeact-mRFPmars and paGFP-Actin or paGFP were seeded onto glass-bottomed dishes 24 hrs prior to imaging and treated with cRGDfV (2.5µM, 2hrs) as indicated. ROI1 was photoactivated and cells were imaged every second for 100s. Normalised intensity was analysed for ROI1 and ROI2 (n=21 (-cRGDfV), n=20 (+cRGDfV)). (B) H1299-Vec and H1299-p53-273H cells transfected as in (A) were seeded onto glass-bottomed dishes 24 hrs prior to imaging. Photoactivation was performed as in (A; n=15 (VEC), n=10 (p53-273H)). (C) MDA-MB-231 cells transfected as in (A) were seeded onto CDM-coated glass-bottomed dishes 4 hrs prior to imaging. Photoactivation was performed as in (A; n=10). Yellow arrows indicate direction of protrusion, error bars represent SEM. All data represent at least 3-independent experiments. Blue bars indicate time points at which -/+cRGDfV or mutant p53 datasets are significantly different ($p<0.01$; Student's T-test).

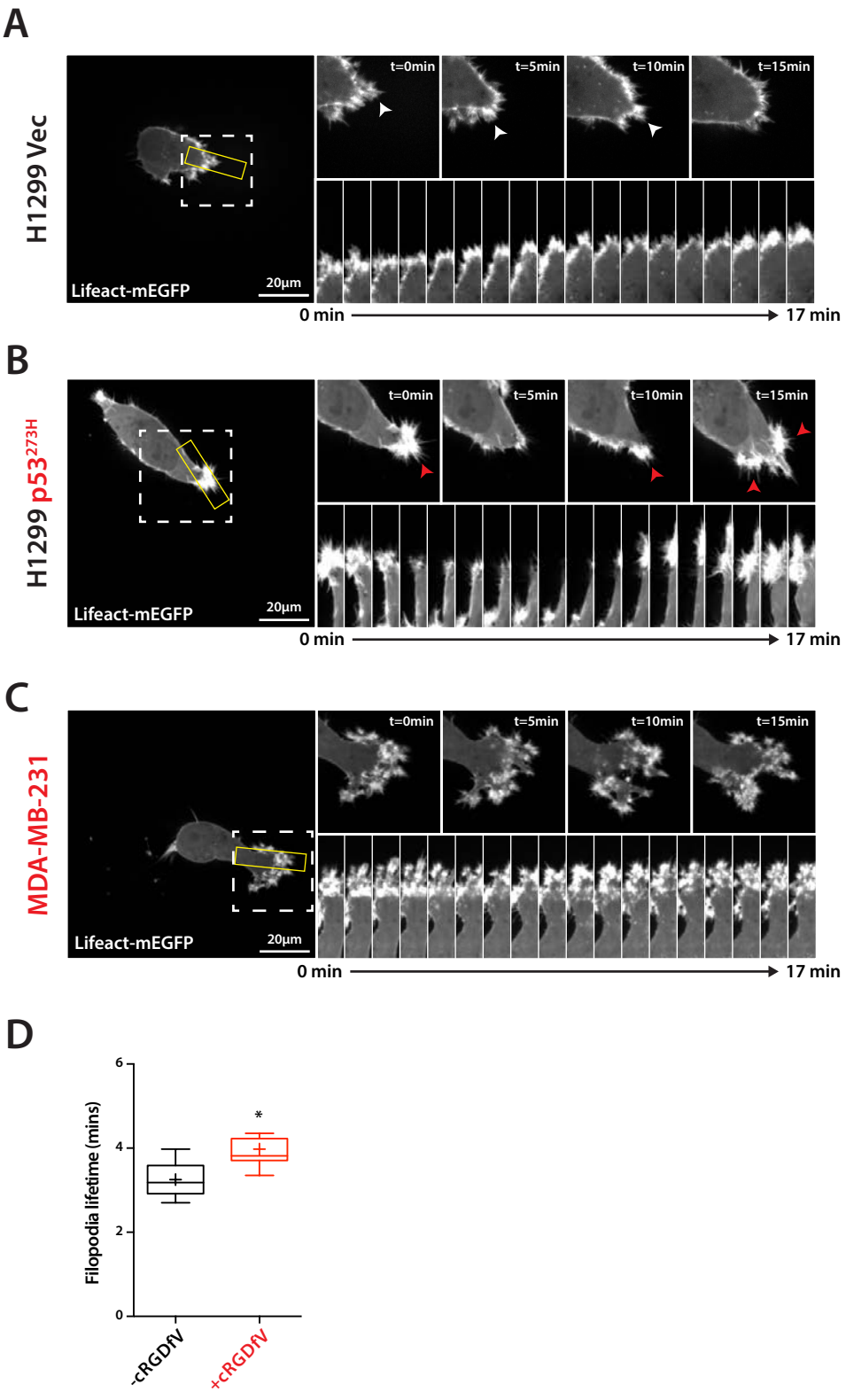

Figure S2: Mutant p53 expressing cells generate bursts of actin spikes.

(A) H1299-Vec, (B) H1299-p53-273H or (C) MDA-MB-231 cells transiently transfected with mEGFP-Lifeact were seeded onto CDMs for 4 hrs and imaged using a spinning disk confocal microscope every minute for >25 mins. Z-projections are shown. White arrows indicate lamellipodial protrusions, red arrows indicate actin spikes. (D) A2780 cells transfected with mEGFP-Lifeact were seeded onto CDMs for 4 hrs and imaged using a spinning disk confocal microscope every minute for 15 minutes and filopodia lifetime was analysed, n=8 cells per condition. All data represent at least 3-independent experiments, statistical significance was evaluated using Student's T-test with Welch's correction. + =mean, * = $p < 0.05$.

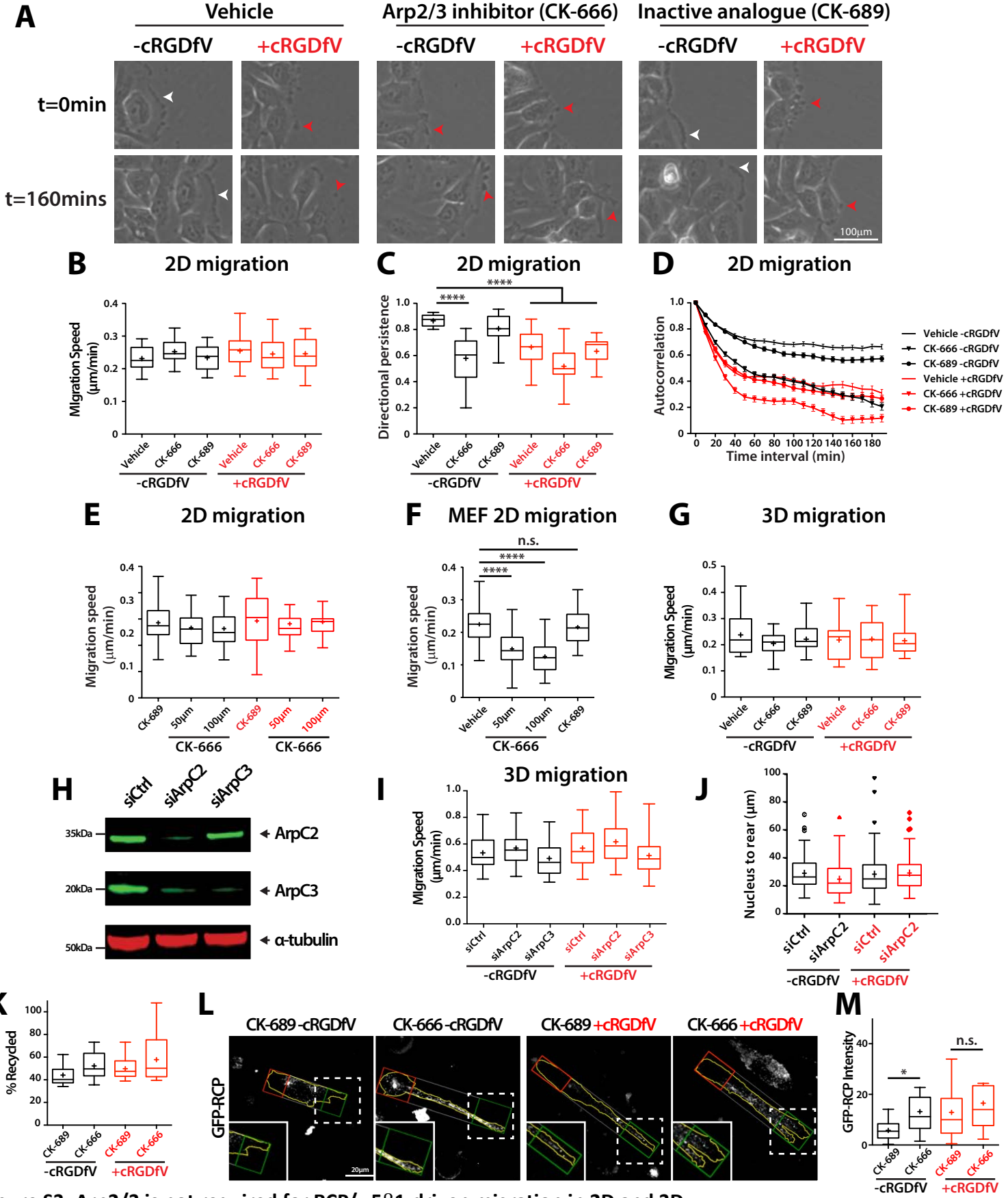

Figure S3: Arp2/3 is not required for RCP/α5β1-driven migration in 2D and 3D.

(A) A2780 cells were seeded onto tissue culture plates 24 hrs prior to wounding. Cells were treated with cRGDfV (2.5µM), DMSO, CK-666 or CK-689 (50µM) as indicated prior to timelapse imaging. White arrows indicate lamellipodia, red arrows indicate non-lamellipodial ruffling protrusions. Migration speed (B), directional persistence (C) and autocorrelation (D) of cells migrating in 2D treated as in (A). n=20 cells per condition. (E) A2780 cells were prepared as in (A) and treated with cRGDfV (2.5µM), DMSO or CK-666 (50µM or 100µM) as indicated prior to timelapse imaging. 2D migration speed was analysed, n=35 cells per condition. (F) Mouse embryonic fibroblasts (MEF) were seeded onto tissue culture plates 24 hrs prior to wounding. Cells were treated withDMSO, CK-689 (100 µM) or CK-666 (50µM or 100µM) as indicated prior to timelapse imaging. 2D migration speed was analysed, n=75 cells per condition. (G) A2780 cells were seeded onto CDM for 4 hrs and treated with cRGDfV (2.5µM) and DMSO, CK-666 or CK-689 (50µM) as indicated prior to timelapse imaging. 3D migration speed was analysed. n=20 cells per condition. (H) siRNA SMARTpool knockdown of ArpC2 and ArpC3 in A2780 cells. (I) 3D migration speed of siCtrl, siArpC2 and siArpC3 A2780 cells migrating in CDM (as in Figure 3C). n≥99 cells per condition. (J) Distance from the rear of the cell to the centre of the nucleus of siCtrl and siArpC2 A2780 cells migrating in CDM. n=100 cells per condition. (K) α5 integrin recycling in A2780 cells was measured upon treatment with CK-666 or CK-689 (50µM), n=24 wells over 3 experiments. (L) GFP-RCP transfected A2780 cells were seeded onto CDMs for 4 hours prior to treatment with cRGDfV (2.5µM), CK-666 or CK-689 (50µM) as indicated prior to confocal imaging. Bounding boxes around the cell perimeter (yellow) were used to identify the front and rear quarter (green or red, respectively) of the cell, and % GFP-RCP intensity at the front measured (M), n=15-28 cells per condition. All data represent at least 3-independent experiments, statistical significance was evaluated using ANOVA/Tukey's multiple comparison test. + = mean. n.s. = not significant, *=p<0.05, **=p<0.01, ***=p<0.001, ****=p<0.0001.

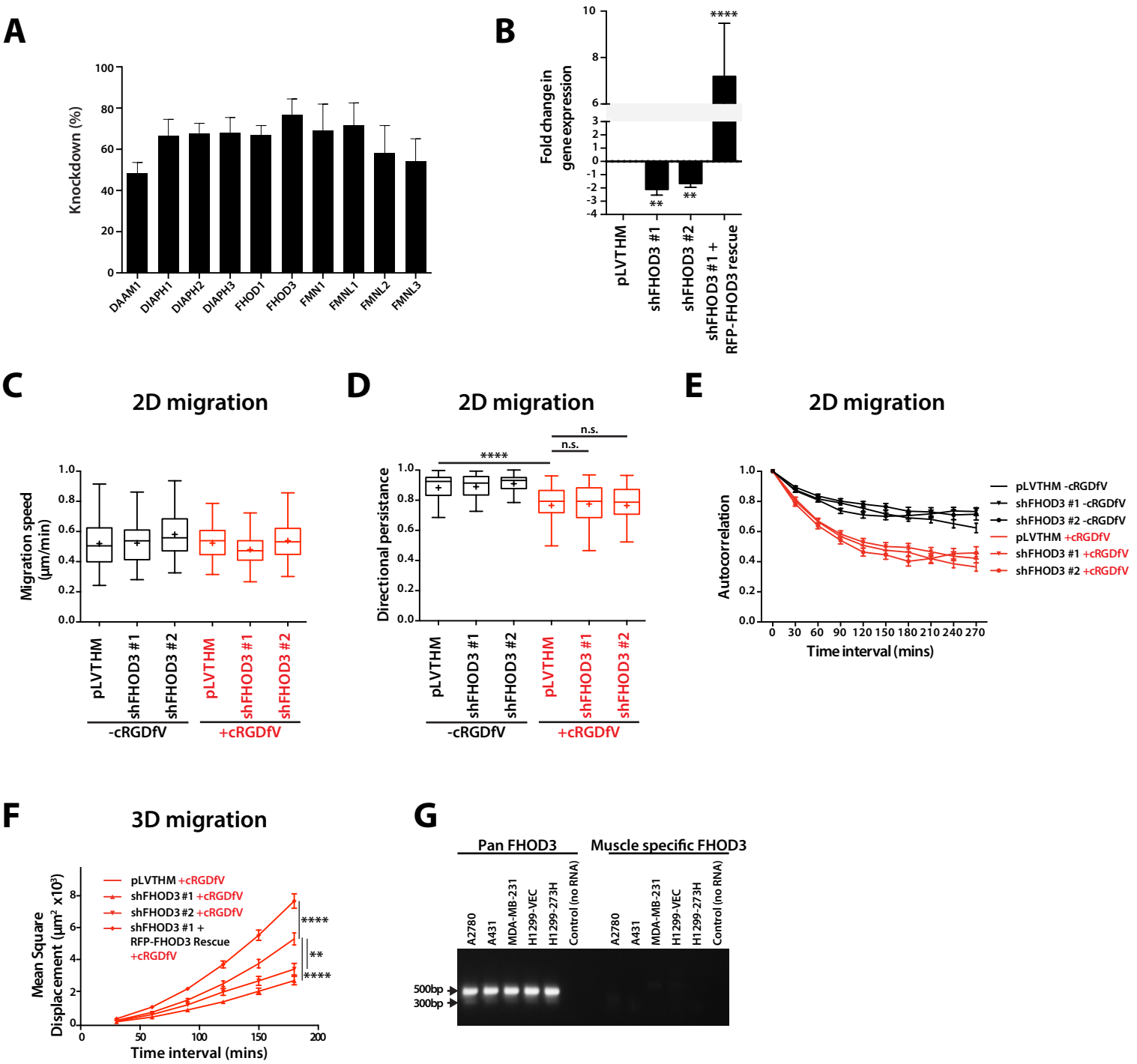

Figure S4: FHOD3 is required for 3D (but not 2D) migration.

(A) Percentage knockdown of formins expressed in A2780 cells by siRNA, measured by qRT-PCR. n=2-3 per condition. (B) A2780 cells were stably transfected with pLVTHM vector control, shFHOD3 #1 or shFHOD3 #2. shFHOD3 #1 was rescued with sh-resistant RFP-FHOD3. FHOD3 gene expression was measured by qRT-PCR. Fold change in gene expression relative to pLVTHM vector control. n=3-6 independent experiments. (C) A2780 cells stably expressing pLVTHM vector control, shFHOD3 #1 or shFHOD3 #2 were seeded onto tissue culture plates 24 hrs prior to wounding. Cells were treated with cRGDfV (2.5µM) as indicated prior to timelapse imaging. Quantification of 2D migration speed, (D) directional persistence and (E) autocorrelation, n=45-70 cells per condition. (F) A2780 cells stably expressing shFHOD3 #1, shFHOD3 #2, pLVTHM vector control or RFP-FHOD3 rescue were seeded onto CDM and treated with cRGDfV (2.5µM) where indicated prior to timelapse imaging, and mean square displacement (MSD) was quantified; n=96-134 cells per condition. (G) RNA extracted from cell lines as indicated was used as to determine FHOD3 isoforms expressed by RT-PCR, using primers specific for non-muscle and muscle specific isoforms of FHOD3 (pan FHOD3, to yield products at 478bp and 502bp respectively) or muscle specific FHOD3 primers (to yield a product at 316bp). All data represent at least 3-independent experiments, statistical significance was evaluated using ANOVA/Tukey's multiple comparison test. + = mean, n.s. = not significant, **=p<0.01, ****=p<0.0001.

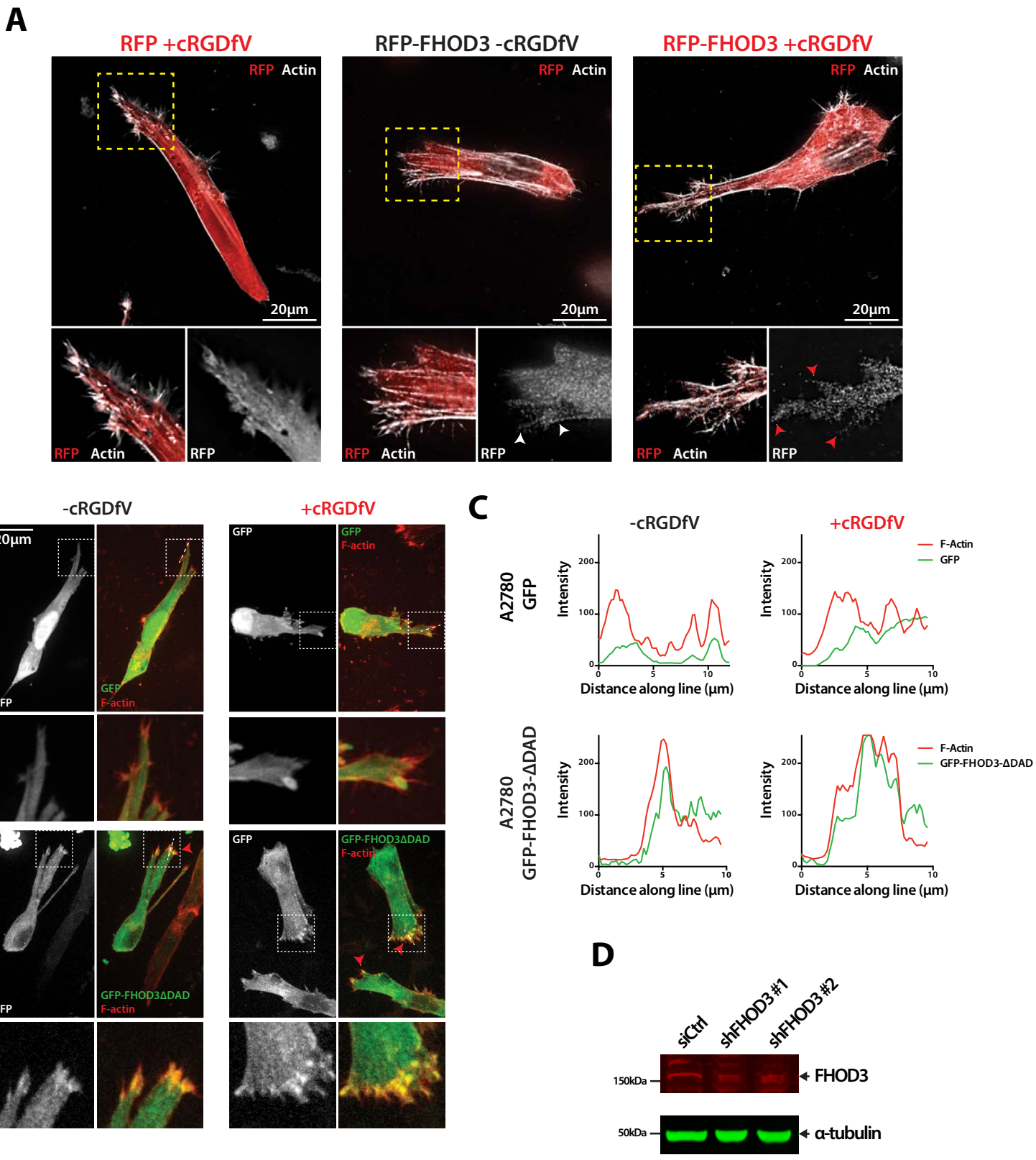

Figure S5: Wild-type FHOD3 localises to actin filaments in 3D CDM; active FHOD3 localises to actin spikes in 3D CDM.

(A) A2780 cells stably expressing RFP or RFP-FHOD3 were seeded onto CDMs for 4 hours and treated with cRGDfV (2.5µM) where indicated. Cells were fixed and stained with anti-RFP antibody and Alexa Fluor 647-conjugated-phalloidin prior to widefield fluorescence imaging. Arrows indicate localisation of RFP-FHOD3 on actin filaments. (B) A2780 cells were transiently transfected with GFP or GFP-FHOD3ΔDAD, seeded onto CDMs for 4 hours and treated with cRGDfV (2.5µM) where indicated. Cells were fixed and stained with TRITC-phalloidin prior to spinning disk confocal imaging. Arrows indicate colocalisation of actin spikes and GFP-FHOD3ΔDAD. Dashed lines indicate line profile intensity measurements in (C). (D) H1299-273H cells were stably transfected with pLVTHM vector control, shFHOD3 #1 or shFHOD3 #2. Cells were lysed; lysates were subjected to SDS-PAGE and Western blotting using antibodies specific for FHOD3 and α-tubulin. All data represent at least 3-independent experiments.